Site-directed mutagenesis study of host and viral proteins: single nucleotide variants of human TBK1 and functional sites of ebolavirus VP35

(部位特異的変異導入法による宿主およびウイルス蛋白質の研究：ヒト TBK1 の一塩基多型とエボラウイルス VP35 の機能的アミノ酸残基)

Nodoka KASAJIMA

Contents

Abbreviations

BDBV	Bundibugyo virus
BOMV	Bombali virus
CTD	C-terminal coiled-coil domain
dbSNP	Single Nucleotide Polymorphism Database
EBOV	Ebola virus
FCS	fetal calf serum
HA	hemagglutinin
HEK	human embryonic kidney
HRTV	Heartland virus
HuH-7	human hepatocellular carcinoma
IFN-I	type I interferon
IFN-β	interferon beta
IID	IFN inhibitory domain
IκB	I-kappa-B
IKKε	IκB kinase-ε
IRF3	IFN regulatory factor 3
ISGs	IFN-stimulated genes
KD	kinase domain
L	large
LLOV	Lloviu virus
M	medium
MAF	minor allele frequency
MARV	Marburg virus
MDBK	Madin-Darby bovine kidney
MDCK	Madin-Darby canine kidney
MLAV	Měnglà virus
MOE	Molecular Operating Environment
NCBI	National Center for Biotechnology Information
NIAID	National Institute of Allergy and Infectious Diseases
NIH	National Institutes of Health
NIID	National Institutes of Infectious Diseases
NP	nucleoprotein
NSs	non-structural

nsSNVs	non-synonymous single-nucleotide variants
PDB	Protein Data Bank
PEI	polyethylenimine
RAVV	Ravn virus
RIG-I	retinoic acid-inducible gene-I
RNA	ribonucleic acid
S	small
SDD	scaffold/dimerization domain
SDS-PAGE	sodium dodecyl sulfate-polyacrylamide gel electrophoresis
SE	standard error
SFTS	severe fever with thrombocytopenia syndrome
SFTSV	severe fever with thrombocytopenia syndrome virus
SK-L	swine kidney L cell.
SNVs	single nucleotide variants
SUDV	Sudan virus
TBK1	TANK-binding kinase 1
TNF-α	tumor necrosis factor-α
ULD	ubiquitin-like domain
VP30	viral protein 30
VP35	viral protein 35
WCL	whole-cell lysates
WT	wild type

Notes

The contents of Chapter II have been published in Viruses.

Kasajima N, Matsuno K, Miyamoto H, Kajihara M, Igarashi M, Takada A. 2021. Functional Importance of Hydrophobic Patches on the Ebola Virus VP35 IFN-Inhibitory Domain. Viruses 13:2316.

Preface

Emerging zoonoses, which accounts for approximately 60% of emerging infectious diseases, are an extensive and growing threat to public health (1–3). Among these zoonoses, viral diseases such as Ebola virus (EBOV) disease cause severe symptoms and high mortality. Severe fever with thrombocytopenia syndrome (SFTS) is also an emerging zoonosis, which was first reported in 2011, and endemic in East Asia. In Japan, 60 to 90 cases are reported every year mostly in the south-western half of the country (4). SFTS is caused by SFTS virus. Treatments and vaccines for EBOV disease and SFTS are currently only limitedly available.

SFTSV and Heartland virus (HRTV), both of which belong to the species *Dabie bandavirus* and *Heartland bandavirus*, respectively, in the genus *Bandavirus*, family *Phenuiviridae*, order *Bunyavirales* (5–7). SFTSV and HRTV found in East Asia and the United States, respectively, are known to be transmitted by ticks and cause acute febrile illness with leukopenia and thrombocytopenia in humans. The case fatality rate for SFTS ranges from 6% to 30%, and several fatal cases have also been reported in HRTV infection (8–10).

SFTSV and HRTV have the genomic S-segment-derived non-structural (NSs) protein (11). The NSs protein acts as an antagonist against type I interferon (IFN-I) induction by targeting the host TANK-binding kinase 1 (TBK1), an essential competent of the signaling pathway of IFN-I production (12). Although serological and genetic surveys demonstrated the prevalence of SFTSV infection in multiple animal species (e.g., goat, sheep, deer, cattle, pig, dog, cat, and chicken) (13, 14), it is unclear whether/how TBK1 of nonhuman animal species are functionally affected by the NSs protein. In addition to this genetic variation of TBK1 among animal species, it also remains elusive whether genetic polymorphisms including non-synonymous single-nucleotide variants (nsSNVs) of human TBK1 affect the antagonism of IFN response and/or severity of SFTSV infection. A previous study reported the genetic polymorphisms in the promoter region of human tumor necrosis factor-α (TNF-α) were involved in the pathogenesis of SFTSV infection (15). Since TBK1 is a direct target of the SFTSV NSs protein, it might be possible that the human TBK1 polymorphisms affect the disease outcome of SFTSV infection due to the altered IFN response.

EBOV belongs to the genus *Ebolavirus* in the family *Filoviridae*. EBOV disease is a severe acute infectious disease with high mortality ranging from 25% to 90% (16). It has been suggested that cytokine storm which represents hyperactive innate immune responses, and on the contrary, suppression of adaptive immune responses are the main pathogenic features of EBOV disease and its lethal outcome (17). Viral protein 35 (VP35)

of EBOV is a multifunctional protein that mainly acts as a viral polymerase cofactor and an interferon antagonist (18, 19). VP35 is composed of 2 major domains, the N-terminal coiled-coil domain and C-terminal IFN inhibitory domain (IID) (20, 21). IID of VP35 interacts with the viral nucleoprotein (NP) and double-stranded RNA for viral RNA transcription/replication and inhibition IFN-I production, respectively (21–23). Previous studies have also identified some regions on IID, which are important for VP35 function, using an alanine substitution approach (21, 22). However, it was indeed unclear whether these alanine substitutions fully altered the VP35 functions and whether the overall stability/structure of the molecule was unchanged by each substitution.

In this study, I performed site-directed mutageneses to analyze amino acid residues important for protein function, focusing on TBK1 and EBOV VP35. The present thesis consists of two chapters. In Chapter I, inhibitory effects of the SFTSV NSs protein on TBK1-mediated IFN induction was compared among various animal species. I first found that the IFN-β promotor activity induced by the transient expression of chicken TBK1 was not impaired by the expression of the SFTSV NSs protein whereas it was significantly inhibited in the cells expressing TBK1 orthologues derived from mammalian species including humans. Then, I generated nsSNVs of human TBK1 and evaluated their permissiveness of TBK1 to the IFN-inhibitory ability of SFTSV and HRTV NSs proteins. The results suggest the possibility that TBK1 polymorphisms including nsSNVs influence the bandavirus NSs protein function as an IFN-I antagonist.

In Chapter II, I analyzed the physical properties of the surface of the VP35 IID molecule, focusing on hydrophobic patches, which are expected to be functional sites to interact with other molecules. Based on the known structural information of VP35 IID, three hydrophobic patches were identified on its surface and their biological importance was investigated using minigenome and IFN-β promoter reporter assays. Site-directed mutagenesis revealed that some of the amino acid substitutions that were predicted to disrupt the hydrophobicity of the patches significantly decreased the efficiency of viral genome replication/transcription due to the reduced interaction with NP, suggesting that the hydrophobic patches on VP35 IID are critical for the formation of a replication complex through the interaction with NP. It was also found that the hydrophobic patches were involved in the IFN-inhibitory function of VP35. These results highlight the importance of hydrophobic patches on the surface of EBOV VP35 IID and also demonstrate that patch analysis is useful for the identification of amino acid residues that directly contribute to protein functions.

Chapter I:
Polymorphisms of TANK-binding kinase 1 affecting interferon-inhibiting activity of bandavirus non-structural proteins

Introduction

SFTSV and HRTV were first identified in China in 2009 and in the United States in 2012, respectively (8, 11). SFTSV and HRTV belong to the species *Dabie bandavirus* and *Heartland bandavirus*, respectively, in the genus *Bandavirus*, family *Phenuiviridae*, order *Bunyavirales* (7). These emerging viruses are mainly transmitted by tick bites and cause fatal diseases in humans (5, 6). Clinically, SFTSV infection often results in acute inflammatory responses accompanied by abnormal induction of immune and inflammatory cytokines in patients' sera (23). While they cause serious diseases with various outcomes from severe and fatal disease to asymptomatic infection, the case mortality rate has been reported as 6-30%, and 0.1%-0.6% subclinical infection of SFTSV in humans has also been observed (24, 25). SFTSV-specific drugs and vaccines are currently unavailable.

Like other phenuiviruses, the SFTSV and HRTV genome consists of three-segmented single-stranded RNA; large (L), medium (M), and small (S). The L and M segments are of negative polarity, which encode the RNA-dependent RNA polymerase and glycoproteins, respectively. On the other hand, the S segment encodes the nucleocapsid protein and the NSs protein with an ambisense strategy (11). Some previous studies have demonstrated that NSs proteins of SFTSV and HRTV antagonize the IFN-I-inducing signal via the retinoic acid-inducible gene-I (RIG-I) cascade by targeting the downstream kinases TBK1/IκB kinase-ε (IKKε) (12, 26, 27). TBK1 mediates the activation of IFN regulatory factor 3 (IRF3), leading to the induction of IFN-I (IFN-α/β) following viral infections. TBK1 is an 84 kDa (729-amino acid) protein containing 4 domains; N-terminal kinase domain (KD), ubiquitin-like domain (ULD), scaffold/dimerization domain (SDD) and C-terminal coiled-coil domains (CTD) (Figure 1A and B)(28, 29). In fact, IFNs are almost undetectable in the blood during the course of SFTSV infection in humans (30). While both SFTSV and HRTV NSs proteins target TBK1, they associate with different domains of TBK1: the SFTSV NSs protein interacts with the KD region (31) and the HRTV NSs protein requires the interaction with the SDD region (32).

Besides the host species difference, single nucleotide variants (SNVs) have also been found to alter susceptibility to infectious diseases. For example, in the case of bandaviruses, TNF-α gene polymorphisms found in the promoter region were reported to

contribute to the severity of SFTS in Chinese Han population (15). In general, the identification of SNVs potentially involved in the permissiveness or resistance to viral infections has been conducted so far by statistical comparative analysis of whole genome sequences of patients and uninfected individuals. On the other hand, there are few studies to experimentally clarify molecular mechanisms by which SNVs are involved in viral pathogenesis. In addition, to know the impact of SNVs, which are infrequent in the global population, molecular studies to identify disease-associated SNVs are needed.

Here, I investigated the anti-IFN-I effect of SFTSV and HRTV NSs proteins on the IFN-production signaling induced by the TBK1 molecule, focusing on genetic polymorphisms in TBK1. It was found that chicken TBK1 was resistant to the SFTSV NSs protein-induced IFN antagonism and that some TBK1 nsSNVs tested in this study retained the function to induce the signaling even in the cells expressing SFTSV and HRTV NSs proteins. The present data demonstrate that bioinformatic approaches with SNV data available on public databases in combination with biological assays could be useful resource for identifying molecular determinants that are potentially associated with pathogenesis of virus infections.

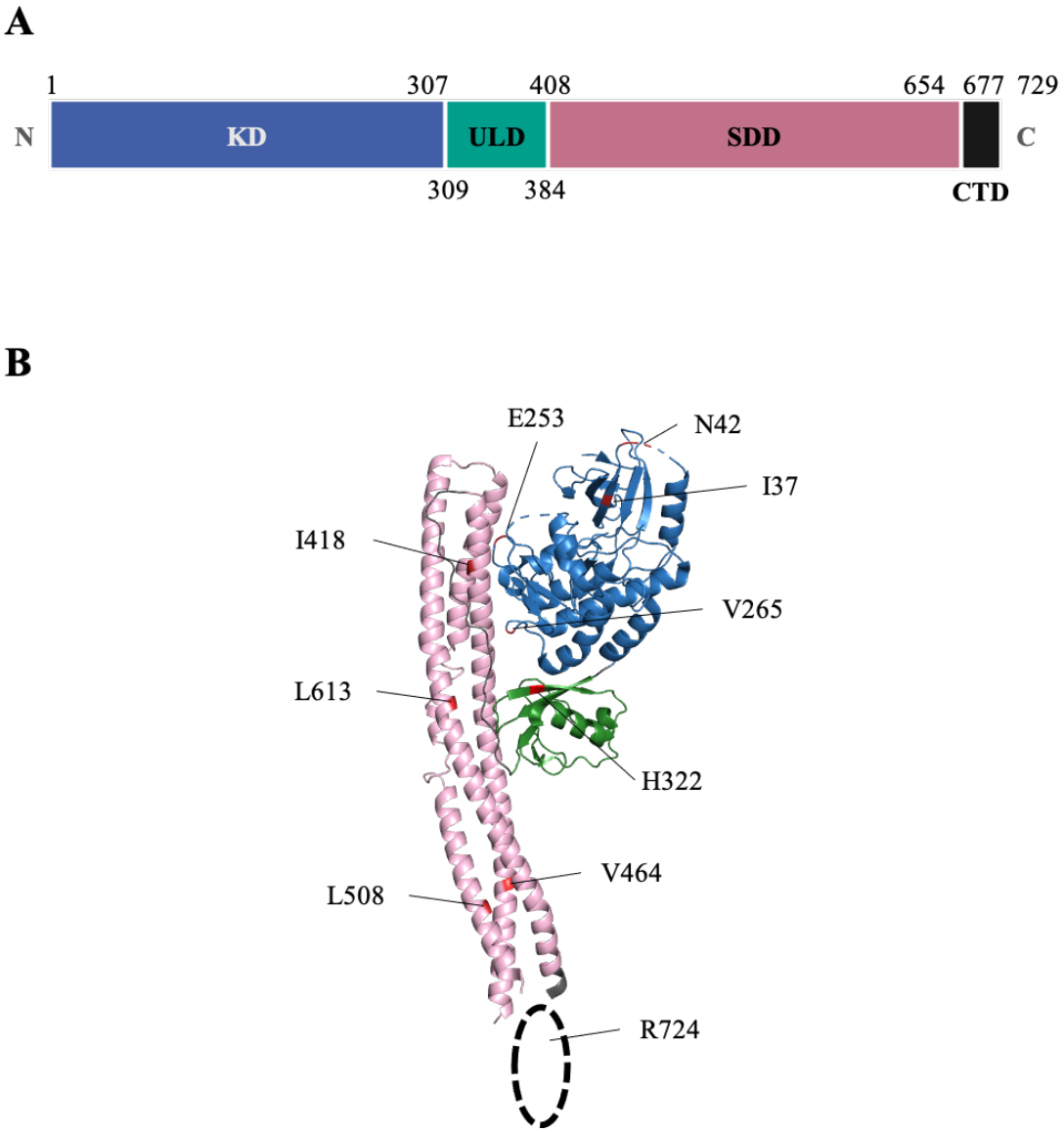

Figure 1. TBK1 protein structure.

(A) Schematic diagram of major domains of the TBK1 protein. TBK1 has the N-terminal serine/threonine protein KD (residues 1-307), the ULD (residues 309-384), the SDD (residues 408-654), and the CTD (residues 677-729). (B) Structural model of TBK1 KD, ULD, and SDD regions (PDB ID: 6NT9 (33)). Blue, green, and pink ribbons represent KD, ULD, and SDD regions, and red residues represent the positions of the amino acid tested in this study. The crystal structure of CTD is not available.

Materials and Methods

Cell culture

Human embryonic kidney (HEK) 293 (ATCC1 CRL-1573™) cells and human hepatocellular carcinoma (HuH-7) cells were grown in Dulbecco's modified Eagle's medium supplemented with 10% fetal calf serum (FCS). Cells were incubated in a humidified 5% CO_2 incubator at 37˚C.

SNV selection

nsSNV substitutions located in the coding region of TBK1 were identified using the Single Nucleotide Polymorphism Database (dbSNP) on the National Center for Biotechnology Information (NCBI) website (data retrieved June, 2019) (34), and nsSNVs used for the site-directed mutagenesis were selected based on the following criteria: (i) nsSNVs with known minor allele frequency (MAF) that are more than 0.001, (ii) nsSNVs that are located in the KD and SDD regions and substitute amino acid residues identical to those found in chicken TBK1.

Construction of plasmids

To construct TBK1-expressing plasmids, total intracellular RNA was extracted from HuH-7 cells, Madin-Darby bovine kidney (MDBK) cells, swine kidney (SK-L) cells, Madin-Darby canine kidney (MDCK) cells, straw-coloured fruit bat spleen cells (ZFBS13-75A), and primary cultures of chick embryo fibroblasts using TRIzol Reagent (Thermo Fisher Scientific). mRNA was prepared using SuperScript III First-Strand Synthesis System and oligo(dT_{20}) (Thermo Fisher Scientific) according to the manufacturer's instructions. Then, cMyc-tagged TBK1 were cloned into the mammalian expression vector pCAGGS (17). Plasmids expressing SFTSV or HRTV NSs-FLAG and a plasmid expressing the activated mutants of RIG-I (RIG-IN) were kindly provided by Dr. Hideki Ebihara (NIID, Japan) and Dr. Sonja Best (NIAID, USA), respectively. Generation of the recombinant plasmids and proteins was approved by Hokkaido University Safety Committee for Genetic Recombination Experiments (21[4]).

Immunoprecipitation assay

HEK293 cells were transfected with the pCAGGS plasmids encoding FLAG-tagged NSs proteins and cMyc-tagged TBK1 using the polyethylenimine (PEI) reagent. At 24 hours after transfection, the cell lysates were prepared with cold lysate buffer (50 mM Tris-HCl, pH 8.0, 150 mM NaCl, 2 mM EDTA, 10% glycerol, and 0.05% NP-40) containing EDTA-free protease inhibitors (Roche). The cell lysates were subsequently

mixed with EZview Red Anti-FLAG Affinity Gel beads (Sigma) and incubated at 4˚C overnight with gentle rocking. After washing with lysate buffer, precipitated proteins were subjected to sodium dodecyl sulfate-polyacrylamide gel electrophoresis (SDS-PAGE) and Western blot analyses with an anti-FLAG monoclonal antibody (600-401-383, ROCKLAND) diluted at 1:1000 and anti-TBK1 antibody (#3504S, Cell Signaling Technology) diluted at 1:1000. The bound antibodies were visualized using Immobilon Western (Millipore). Band intensities were quantified using Amersham Imager 600 Analysis Software.

IFN-β promoter reporter assay

HEK293 cells (3 x 10^5) on 24-well plates were transfected with the RIG-IN- or cMyc-tagged TBK1-expressing plasmids and the plasmids for the expression of the human IFN-β promoter-driven firefly luciferase reporter gene (pIFNβ-luc., kindly gifted by Sonja Best, NIH/NIAID) and of the Renilla luciferase gene cloned into pRL-TK vector (Promega) along with or without the plasmid expressing the SFTSV or HRTV NSs protein (IFN-antagonist). The cells were lysed in Passive Lysis Buffer (Promega), and then luciferase assays were performed using the Dual-Luciferase Reporter Assay System (Promega) according to the manufacturer's directions. Firefly luciferase values were normalized to Renilla luciferase values. Normalized values were then compared to negative control (i.e., conditions without induction by the expression of RIG-IN or human wildtype TBK1) to obtain fold induction values. Generation of the recombinant plasmids and proteins was approved by Hokkaido University Safety Committee for Genetic Recombination Experiments (21[4]).

Statistical analysis

Statistical analyses were carried out using Dunnett's multiple-comparison test implemented in R (35). Significance was defined as a *p*-value using the following notations: $*p < 0.05$, $**p < 0.01$, $***p < 0.001$, $****p < 0.0001$.

Results

Suppression of IFN production induced by TBK1 derived from various animal species

To compare the effect of the expression of the SFTSV NSs protein on TBK1-mediated IFN-production signaling among animal species, the IFN-β promoter activity induced by the expression of TBK1 from various animal species were analyzed in the cells expressing the SFTSV NSs protein (Figure 2). The mammalian and chicken TBK1 genes were cloned into the expression plasmid and transfected into HEK293 cells together with reporter plasmids. It was confirmed that all the TBK1 orthologues tested, including chicken TBK1, induced IFN-production signaling in this human cell line (Figure 3A). As expected, the reporter activities in the cells expressing mammalian TBK1 (i.e., human, bovine, swine, canine, and bat) were significantly reduced by co-expression of the SFTSV NSs protein (Figure 3B). In contrast, the reporter activity was not impaired by the expression of the SFTSV NSs protein in the cells expressing chicken TBK1. To confirm the interaction between the SFTSV NSs protein and TBK1, immunoprecipitation assay was carried out using HEK293 cells transfected with the pCAGGS plasmids encoding FLAG-tagged NSs protein and cMyc-tagged TBK1 (Figure 4). As well as human TBK1, TBK1 derived from various mammalian species were also co-immunoprecipitated with the SFTSV NSs protein. Unexpectedly, chicken TBK1 whose signaling function was not suppressed by the SFTSV NSs protein, was also co-immunoprecipitated with the NSs protein.

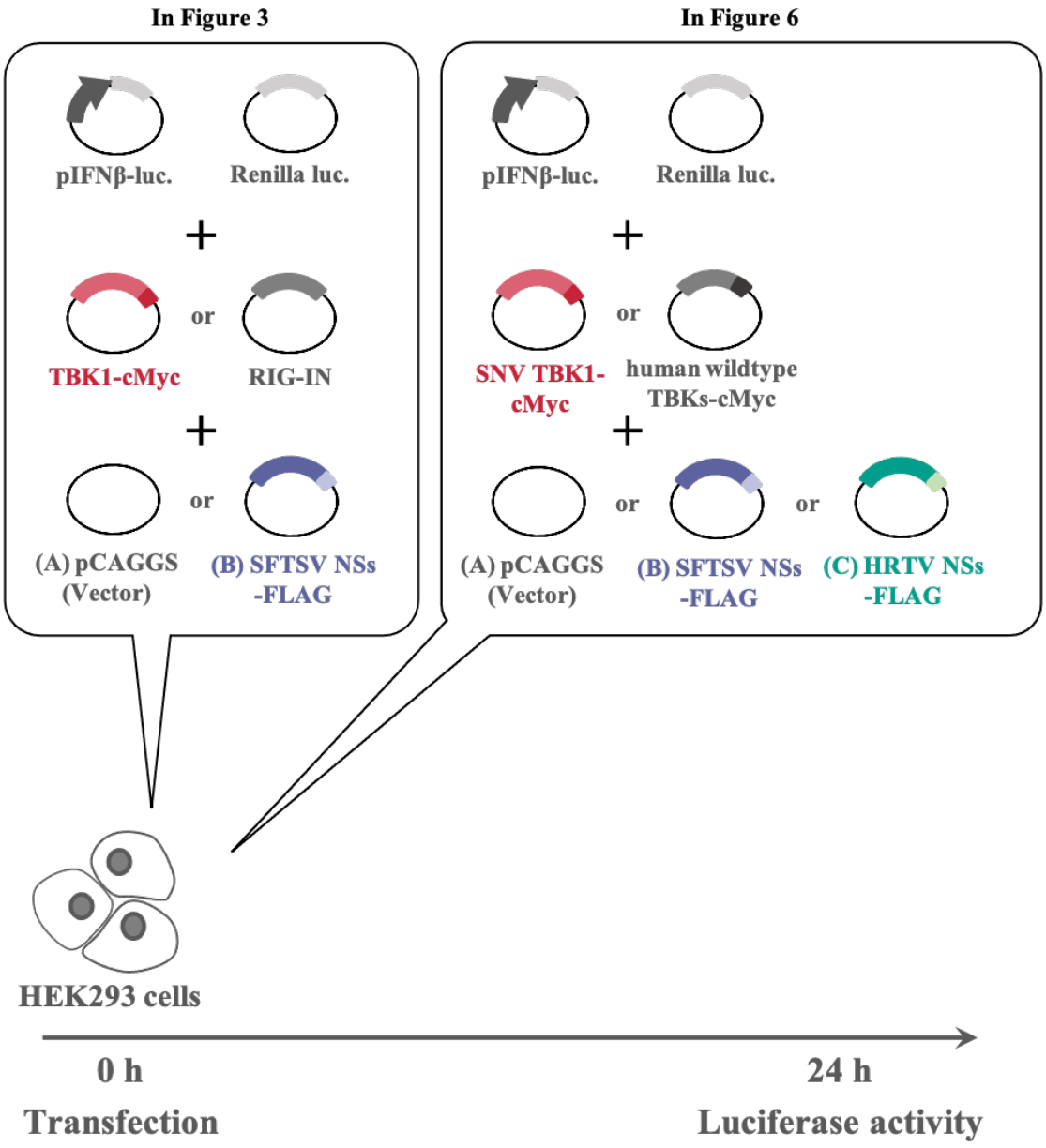

Figure 2. Schematic diagram of IFN-β promoter reporter assays.

HEK293 cells were transfected with the plasmids expressing the reporter genes, TBK1 or RIG-IN as a control, along with or without NSs-expressing plasmid, and luciferase activities under the control of the IFN-β promoter were measured at 24 h post-transfection.

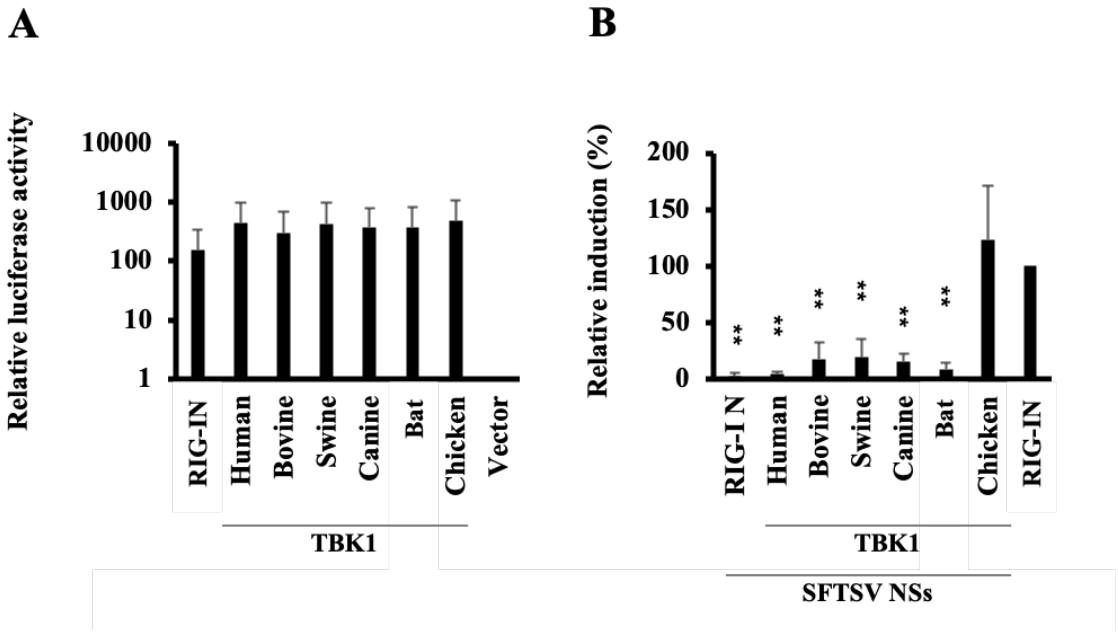

Figure 3. Relative IFN-β promoter activity induced by TBK1 of different animal origins.

HEK293 cells were transfected with the plasmids expressing the reporter genes, TBK1 or RIG-IN (A). HEK293 cells were transfected with above-mentioned plasmids together with that expressing the SFTSV NSs protein (B). The fold activation compared with the vector-transfected cells (A) and the relative induction compared with RIG-IN plasmid-transfected cells without the expression of SFTSV NSs (B) are shown. The origin of each TBK1 gene was indicated on the bottom. Data are presented as means ± standard error (SE) (n = 3). Dunnett's multiple-comparison test was used for the comparison to RIG-IN in the absence of the NSs protein. $^{**}p < 0.005$.

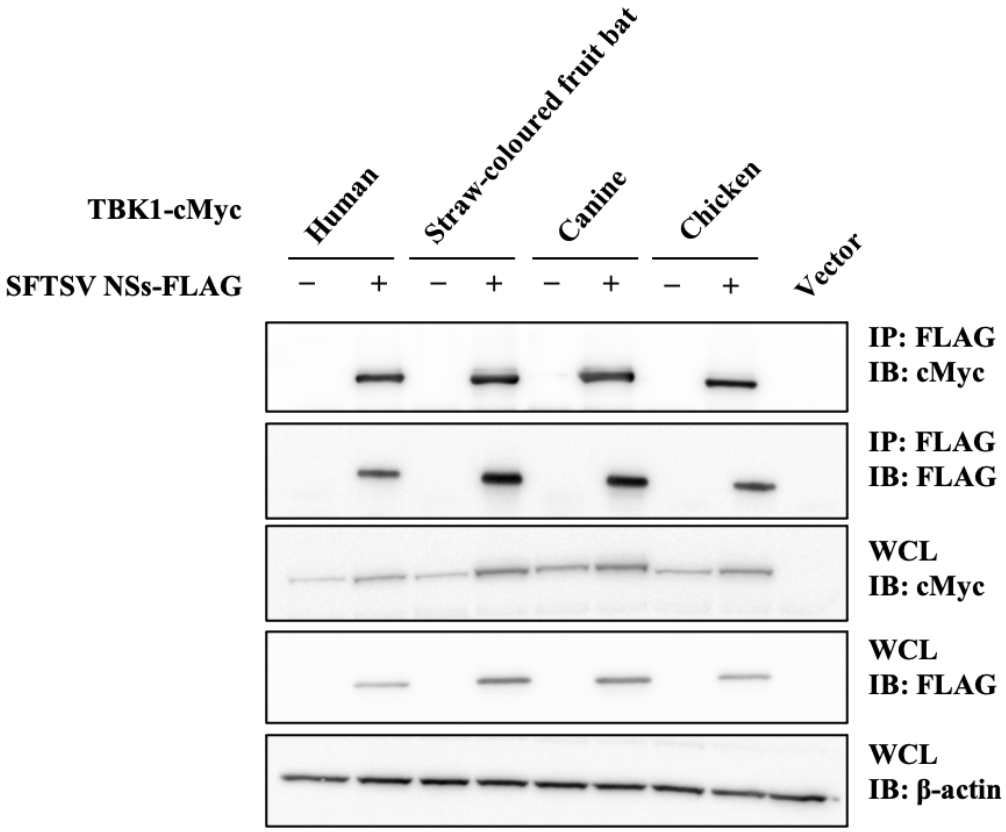

Figure 4. Immunoprecipitation of TBK1 and NSs protein.

HEK293T cells were transfected with the plasmids expressing TBK1-cMyc and/or SFTSV NSs-FLAG. Following lysis of the cells, SFTSV NSs was immunoprecipitated (IP) using anti-FLAG antibodies. Each protein was visualized by immunoblotting using anti-FLAG and anti-cMyc antibodies for both IP samples and whole-cell lysates (WCL).

SNV profile of human TBK1

I then investigated nsSNVs of human TBK1. According to the SNVs information collected from NCBI SNP database (dbSNP), at least 368 nsSNVs are present in the human TBK1 gene (data not shown). Among them, I conducted subsequent experiments focusing on the ten selected nsSNVs (Table 1). First, five nsSNVs with MAF of 0.001 or higher were selected. These SNVs cause the following amino acid substitutions. H322Y, V464A, L508I, L613F, and R724C were located outside of the KD region important for the interaction with the SFTSV NSs protein. V464A, L508I, and L613F were located in the SDD region which is important for the interaction with the HRTV NSs protein. In addition to these five nsSNVs selected by focusing on MAF, other five nsSNV substitutions were selected by the sequence comparison with chicken TBK1 (Figure 5) since chicken TBK1-mediated IFN-production singling was not inhibited by the expression of SFTSV NSs proteins (Figure 3B). These nsSNV TBK1 (I37V, N42S, E253A, V265I, and I418V in the KD or SDD region) have amino acid residues that are the same as those of chicken TBK1 at the respective positions (Figure 5).

Table 1. Amino acid substitutions and frequencies of TBK1SNVs examined in this study.

dbSNP ID	AA substitution	Alleles	MAF	Domain
rs780879936	I37V	A to G	$< 10^{-4}$	KD
rs748061846	N42S	A to G	$< 10^{-4}$	
rs767796656	E253A	A to C	$< 10^{-5}$	
rs780177120	V265I	G to A	$< 10^{-4}$	
rs145905497	H322Y	C to T	0.001	ULD
rs138839127	I418V	A to G	$< 10^{-4}$	SDD
rs35635889	V464A	T to C	0.004	
rs144424516	L508I	C to A	0.003	
rs368859659	L613F	G to T	0.002	
rs185524052	R724C	C to T	0.001	CTD

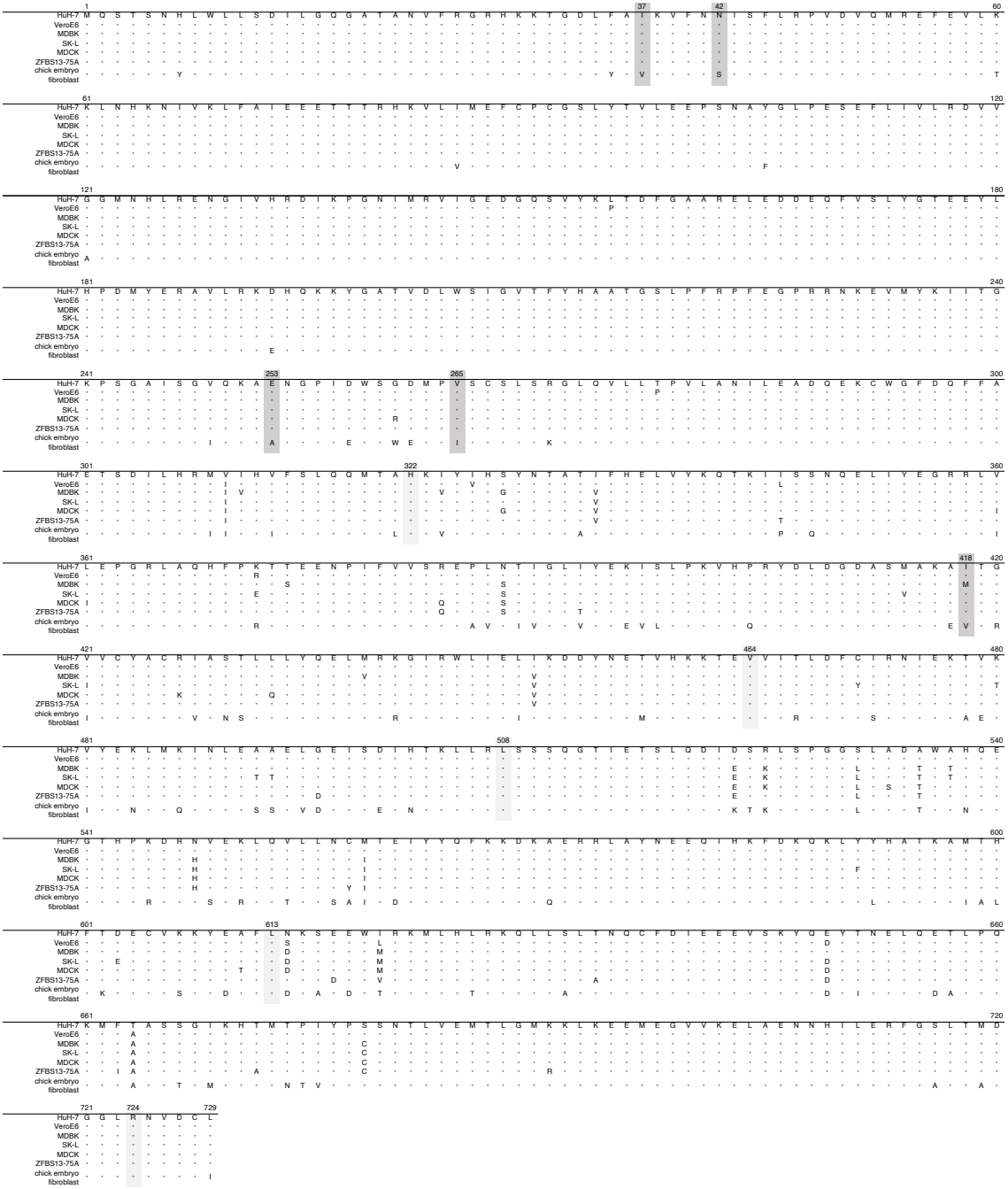

Figure 5. Multiple alignment of TBK1 amino acid sequences.

TBK1 amino acid sequences of different animal species are shown; human (HuH-7), monkey (Vero E6), bovine (MDBK), swine (SK-L), canine (MDCK), bat (ZFBS13-75A), and chicken. Highlighted are the amino acid positions tested in this study. Dark gray highlight represents the SNV positions selected for the mutagenesis based on the amino acid difference between chickens and humans.

IFN-β-inducing capacity of wildtype and mutant TBK1 with nsSNV substitutions

It was previously shown that nsSNVs of an IFN-inducing factor (i.e., RIG-I) had an impaired capacity for IFN production (36). Therefore, to confirm the IFN-inducing ability of the 10 nsSNV mutants of TBK1, the IFN-β promoter reporter assay was carried out (Figures 2 and 6A). As previously reported, the exogenous expression of wildtype human TBK1 induced IFN-β promoter activity. It was also confirmed that all the TBK1 mutants with the nsSNV substitutions showed similar levels of the IFN-β promoter activity to that of wildtype human TBK1 (Figure 6A) and there was no statistically significant difference among these TBK1. These data suggested that none of the nsSNV substitutions introduced in this study impaired the signaling ability of TBK1 for the IFN-β promoter activation.

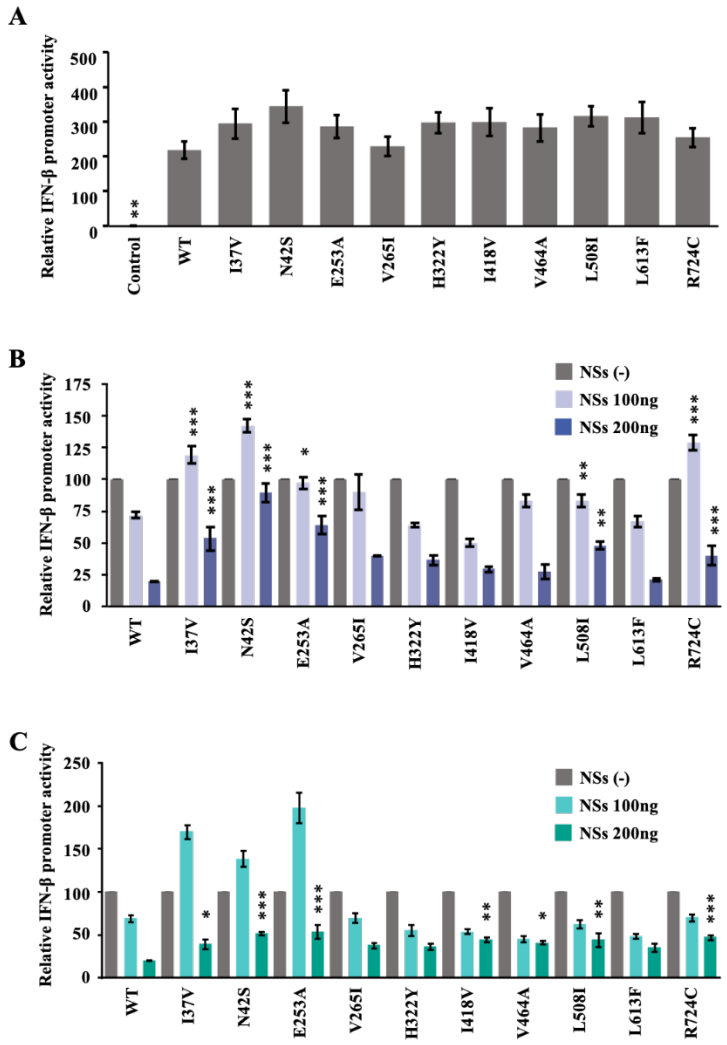

Figure 6. Relative IFN-β promoter activity induced by human SNV TBK1.

(A) HEK293 cells were transfected with an empty vector (Control), wildtype (WT)-, or SNP-introduced TBK1-expressing plasmids, and expression plasmids of Renilla luciferase along with pIFNβ-luc. IFN-β promoter activity was quantified by measuring luciferase, and normalized to the level of expression of Renilla luciferase. Each bar represents mean ± SE from three independent experiments. Dunnett's multiple-comparison test was used for the comparison to WT (**$p < 0.01$). (B, C) The relative IFN-β promoter activity in HEK293 cells co-transfected with the above-mentioned plasmids and that expressing the SFTSV NSs (B) or HRTV (C) NSs protein are shown. The relative IFN-β promoter activity was calculated setting the values of each TBK1 expression alone [NSs (-)] as 100%. Each bar represents mean ± SE from three independent experiments. Dunnett's multiple-comparison test was used for the comparison to WT (*$p < 0.05$, **$p < 0.01$, ***$p < 0.001$).

Effects of TBK1 nsSNV substitutions on the anti-IFN-I function of SFTSV and HRTV NSs proteins

Next, I tested the 10 nsSNV substitutions for the effects on the IFN-β signaling-inhibitory activity of the NSs protein (Figures 2, 6B, and C). As previously reported (32, 37). the IFN-β promoter activity was remarkably reduced when SFTSV and HRTV NSs proteins were expressed together with wildtype human TBK1. On the other hand, nsSNVs with I37V, N42S, E253A, L508I, or R724C substitution induced significantly higher IFN-β promoter activity than wildtype human TBK1 in the presence of the SFTSV NSs protein (Figure 6B). This suggested that these amino acid substitutions altered the permissiveness of TBK1 to the SFTSV NSs protein function as an IFN-I antagonist. The nsSNV substitutions in the KD region (I37V, N42S, and E253A) had the significant impact on the resistance of TBK1 to the inhibition of signaling activity by the SFTSV NSs protein. In the same way, effects of the nsSNV substitutions of TBK1 against the HRTV NSs protein were evaluated (Figure 6C). It was found that I37V, N42S, E253A, I418V, V464A, L508I, and R724C substitutions resulted in significantly higher IFN-β promoter activation than wildtype human TBK1 in the cells co-expressing the HRTV NSs protein, although the impact of I37V and V464A was relatively slight (Figure 6C). The nsSNV substitutions in the SDD region (I418V, V464A, and L508I) had impact against the HRTV NSs protein, whereas no significant difference from wildtype human TBK1 was found in nsSNV with the L613F substitution, which was also located in this domain. The significant impact of the nsSNV substitutions I418V and V464A were only found against the HRTV NSs protein. Interestingly, some nsSNV substitutions (L508I and R724C for SFTSV NSs: I37V, N42S, E253A, and R724C for HRTV NSs), which were located in the domains other than the respective interaction sites of SFTSV and HRTV NSs proteins, were also found to affect the ability of the NSs protein to suppress TBK1-mediated IFN-I signaling. These data suggest some unknown mechanisms for the interaction between the NSs proteins and TBK1.

Discussion

It is reported that the inhibition of TBK1-mediated signaling by SFTSV and HRTV NSs proteins is important for pathogenicity of these viruses (30, 32). Previous studies have demonstrated that the target molecule of the NSs proteins is TBK1 in host cells (12, 26, 27). In the present study, I focused on genetic polymorphisms in TBK1 and investigated the difference among animal species and nsSNVs for their permissiveness or resistance to the SFTSV and HRTV NSs protein function as an IFN-I antagonist.

I first found that the IFN-β promotor activation induced by chicken TBK1 was not impaired by the expression of the SFTSV NSs protein whereas it was significantly inhibited in the cells expressing TBK1 of mammalian species tested. A previous study suggested that chicken TBK1, like human TBK1, is ubiquitously expressed in chicken tissues and acts as an important factor for IRF3 activation and IFN-β induction in response to avian leukosis virus infection (38). Chicken and human TBK1 amino acid sequences showed high identity (86.4%). When focusing on the KD region, although the identity of human TBK1 with other animal species (i.e., bovine, swine, canine, and bat,) is almost 100%, chicken TBK1 has relatively low identity to human TBK1 (94.8%). This difference found in the KD region of chicken TBK1 might be responsible for the resistance to the NSs protein function. On the other hand, the immunoprecipitation assay suggested that chicken TBK1 interacted with the SFTSV NSs protein as well as mammalian TBK1. Therefore, some other factors in addition to the interaction with the TBK1 KD region may be required for the suppression of TBK1-mediated signaling by the SFTSV NSs protein.

The present study then focused on nsSNVs of human TBK1. I have identified some TBK1 nsSNVs that were resistant to the NSs protein-induced inhibition of IFN-β promotor activity. As expected, the nsSNV substitutions in the KD and SDD regions, which are known as the interaction sites of SFTSV and HRTV NSs proteins, respectively, were found to affect the IFN-signaling inhibition by the NSs proteins. Interestingly, it was also found that some nsSNV substitutions present outside these interaction sites also showed resistance to the IFN antagonism by the NSs proteins. Furthermore, most of the nsSNV substitutions that affected the IFN-inhibition activity of both SFTSV and HRTV NSs proteins were located in the KD region. Therefore, it is speculated that the IFN-signaling inhibition by the NSs proteins may be closely related to the kinase function of TBK1. These results suggest that the NSs proteins inhibit the TBK1-mediated IFN signaling not only through the interaction of the NSs proteins with the KD and SDD regions but also some other mechanisms. The R724C substitution, which caused resistance to both SFTSV and HRTV NSs protein function, is present in the CTD region. The CTD region is reported to be important for the interaction with some adaptor proteins

(i.e., optineurin and NAK-associated protein 1), which are known to contribute to the IFN production via RIG-I during viral infection (39, 40). Thus, it may be interesting to explore whether the R724C substitution alters the interaction between the adaptor proteins and TBK1.

The present study suggests the possibility that TBK1 polymorphisms affect the IFN antagonism of the bandavirus NSs proteins and could potentially be one of the factors for differences in the severity of SFTSV and HRTV infections. Mechanisms by which TBK1 became resistant to the IFN-inhibition activity of the NSs proteins is not clarified in this study. It would be interesting to examine phosphorylation of TBK1 and IRF3 to determine if their interaction is affected by nsSNV substitutions. In addition, since TBK1 is also a target for other viral proteins such as EBOV VP35, which is also known as an IFN antagonist, it is also of interest to investigate TBK1 nsSNVs resistant to the IFN antagonism of VP35.

Summary

Human-pathogenic tick-borne bandaviruses, SFTSV and HRTV have posed serious threats to public health. The genomic S-segment-derived NSs protein of SFTSV and HRTV act as antagonist against IFN-I induction by targeting the host TBK1, an essential competent of the signaling pathway of IFN-I production. We first found that the IFN-β promotor activity was not impaired by the expression of SFTSV NSs in the cells expressing chicken TBK1 whereas it was significantly inhibited in the cells expressing TBK1 orthologues derived from mammalian species including humans. Then, nsSNVs of human TBK1, which are thought to be an important factor involved in viral pathogenesis, were tested for their permissiveness to SFTSV and HRTV NSs proteins. The nsSNV substitutions I37V, N42S, E253A, L508I, and R724C in human TBK1 were found to reduce the IFN-β signaling-inhibitory activity of SFTSV and HRTV NSs proteins. Interestingly, the nsSNV substitutions I418V and V464A were less resistant to SFTSV than to HRTV NSs proteins. These results suggest the possibility that TBK1 polymorphisms including nsSNVs influence the bandavirus NSs protein function as an IFN-I antagonist and may potentially be one of the factors involved in differences in the severity and/or pathogenesis of SFTSV and HRTV infections.

Chapter II:
Functional importance of hydrophobic patches on the Ebola virus VP35 IFN-inhibitory domain

Introduction

EBOV is an enveloped, negative-stranded RNA virus that belongs to the genus *Ebolavirus* in the family *Filoviridae*. The genus *Ebolavirus* consists of six species represented by EBOV, Sudan virus (SUDV), Taï Forest virus (TAFV), Bundibugyo virus (BDBV), Reston virus (RESTV), and Bombali virus (BOMV) (41, 42). The genus *Marburgvirus*, other principal members of the virus family, includes 2 viruses, Marburg virus (MARV) and Ravn virus (RAVV) in a single species. EBOV, SUDV, TAFV, BDBV, MARV, and RAVV cause hemorrhagic fever in humans and nonhuman primates with high mortality rates of up to 90%, for which clinically approved antivirals and vaccines remain limited (43). In addition, other filoviruses such as Lloviu virus (LLOV) and Měnglà virus (MLAV) have been recently discovered and classified into the genus *Cuevavirus* and genus *Dianlovirus*, respectively, in the family *Filoviridae* (44, 45).

EBOV has a non-segmented RNA genome (approximately 19 kb) encoding three nonstructural and seven structural proteins (46). Among the viral structural proteins, VP35, viral protein 30 (VP30), nucleoprotein (NP), and RNA-dependent RNA polymerase L protein act as essential components of the viral replication complex. EBOV VP35 is also known as an IFN antagonist that interacts with host proteins involved in multiple IFN-production pathways and multiple IFN-stimulated genes (ISGs) (19). VP35-mediated suppression of IFN production involves a variety of host factors: VP35 inhibits IFN production by interacting with TBK1 and IKKε and by suppressing post-translational modifications of IRF3 and 7 (47).

VP35 is composed of 2 major domains, the N-terminal coiled-coil domain and C-terminal IID (20). On one hand, the coiled-coil domain is essential for several VP35 functions, including viral genome replication and nucleocapsid formation (48). On the other hand, IID is required and sufficient for binding to dsRNA, leading to IFN inhibition (49–51). IID has a cluster of conserved basic amino acid residues that are important for dsRNA binding (22). IID is also sufficient to interact with NP (21). Previous studies on the VP35 IID structure have defined two highly conserved basic regions, designated “first basic patch” and “central basic patch”, both of which are important for the VP35 functions (21, 22). The first basic patch consisting of residues K222, R225, K248, and K251 is critical for both polymerase cofactor function and the interaction with NP (21, 52) while

the central basic patch consisting of R305, K309, R312, R319, R322, and K339 is critical for IFN-antagonism (22, 52). Amino acid substitutions in these patches resulted in increased IFN-α/β responses, reduced viral replication, and attenuation of EBOV in animal models (22, 53). Thus, these basic patches in IID are thought to be important for both polymerase cofactor activity and IFN antagonism (21, 54).

Protein patches generally reflect physical properties of molecular surfaces of protein structures and patch analyses are used to predict surface regions involved in protein-protein interactions (55). Among protein patches on protein surfaces defined by physical properties (solvation potential, residue interface propensity, hydrophobicity, planarity, protrusion, and accessible surface area), hydrophobic patches are particularly expected to be functional sites that are involved in interactions with other proteins (55, 56). In the present study, I identified three hydrophobic patches on the IID surface using the 3D structural information of the VP35 molecule (PDB ID: 3FKE). One of the hydrophobic patches was found to be critical for the VP35 function as a viral polymerase cofactor. I further found that a subset of amino acid residues located within this hydrophobic patch was important for the VP35-NP interaction, which is required for formation of the genome replication complex. Furthermore, two of the three hydrophobic patches were also found to be important for the suppression of IFN production by VP35. My data highlight the importance of the IID hydrophobic patches in the principal functions of EBOV VP35.

Materials and Methods

Patch analysis

Protein surface patches of EBOV (Variant Mayinga, species *Zaire ebolavirus*) VP35 IID (PDB code: 3FKE, chain B) were detected using Molecular Operating Environment (MOE) software (version 2018; Chemical Computing Group, Montreal, QC, Canada). Three hydrophobic patches were identified on the VP35 IID structure. To experimentally investigate whether these patches were functionally important, amino acid substitutions that eliminated each hydrophobic patch were determined by computational calculations with MOE. When considering a patch consisting of n residues, $n \times 19$ mutants were generated at each patch by mutating a residue to the other 19 amino acids *in silico*. Then, for these mutants, I calculated the difference in the patch area and thermostability (*dStability*) from wildtype VP35 to each mutant (Table 2-4). Finally, I chose the mutants having the following three characteristics: (i) disappearance of the relevant patch area, (ii) no effects on other patches (i.e., numbers and area), and (iii) *dStability* within 2.0 kcal/mol (Table 5).

Cell culture and construction of plasmids

HEK 293 (ATCC1 CRL-157) and HEK293T cells (ATCC1 CRL-321) were grown in Dulbecco's modified Eagle's medium with 10% FCS. The cells were incubated in a humidified 5% CO2 incubator at 37˚C. The cDNA encoding hemagglutinin (HA)-tagged VP35 of an EBOV variant, Mayinga (species *Zaire ebolavirus*), were cloned into the mammalian expression vector pCAGGS (57) as described previously (58). HA-tagged mutant VP35 genes were also constructed by site-directed mutagenesis using KOD One (Toyobo) and cloned into pCAGGS. The NP, VP35, VP30, VP24, and L genes of EBOV Mayinga were similarly cloned into pCAGGS. An EBOV minigenome plasmid containing the firefly luciferase gene, p3E5E-luc, was constructed as described previously (58, 59).

Minigenome reporter assay

The EBOV minigenome assay was carried out using a previously described system (58, 60). Briefly, HEK293T cells (2×10^5) on 24-well plates were transfected with 50, 100, or 200 ng of plasmids encoding HA-tagged wildtype EBOV VP35, mutant VP35, or the HA tag alone, along with the plasmids for the expression of EBOV NP (50 ng), VP30 (30 ng), L (400 ng), p3E5E-luc (100 ng), and the T7 polymerase (100 ng) using the PEI reagent. At 36 hours after transfection, the cells were lysed with Passive Lysis Buffer (Promega), and the luciferase activity was measured using the Dual-Glo luciferase assay

system (Promega) according to the manufacturer's instructions. These cell lysates were also subjected to SDS-PAGE, followed by western blot analysis to examine the expression of each protein with a monoclonal anti-β-actin antibody (Abcam, ab6276) diluted at 1:5000 and a monoclonal anti-HA antibody (Abcam, ab1424) diluted at 1:5000. The firefly luciferase activity was compared to a negative control (i.e., absence of HA tagged-VP35) to obtain fold luciferase activity values. Generation of the recombinant plasmids was approved by the Ministry of Education, Culture, Sports, Science, and Technology, Japan (元受文科振第 235 号).

Immunoprecipitation assay

HEK293T cells were transfected with the pCAGGS plasmids encoding HA-tagged VP35 and NP using the PEI reagent according to the manufacturer's instructions. At 36 hours after transfection, the cell lysates were prepared with cold lysate buffer (50 mM Tris-HCl, pH 8.0, 150 mM NaCl, 2 mM EDTA, 10% glycerol, and 0.05% NP-40) containing EDTA-free protease inhibitors (Roche). The cell lysates were subsequently mixed with EZview Red Anti-HA Affinity Gel beads (Sigma) and incubated at 4˚C overnight with gentle rocking. After washing with lysate buffer, precipitated proteins were subjected to SDS-PAGE and Western blot analyses with a monoclonal anti-HA antibody (Abcam, ab1424) diluted at 1:5000 and rabbit antiserum to EBOV NP (FS0169) (61) diluted at 1:2000. The bound antibodies were visualized using Immobilon Western (Millipore). Band intensities were quantified using Amersham Imager 600 Analysis Software.

IFN-β promoter reporter assay

HEK293 cells (2 x 10^5) on 24-well plates were transfected with the HA-tagged VP35-expressing plasmid along with the plasmids for the human IFN-β promoter-driven firefly luciferase reporter gene (pIFNβ-luc., kindly gifted by Sonja Best, NIH/NIAID) and for the Renilla luciferase cloned into pRL-TK vector (Promega). Twenty-four hours after transfection, the cells were stimulated with 5 ng/μl poly(I:C) (InvivoGen). The cells were lysed in Passive Lysis Buffer (Promega), and then luciferase assays were performed using the Dual-Luciferase Reporter Assay System (Promega) according to the manufacturer's directions. These cell lysates were subjected to SDS-PAGE, followed by Western blotting, to examine the expression of each protein. Firefly luciferase values were normalized to Renilla luciferase values. Normalized values were then compared to a negative control (no induction by poly(I:C)) to obtain fold induction values. Samples were also used for Western blotting as described above. Generation of the recombinant

plasmids and proteins was approved by Hokkaido University Safety Committee for Genetic Recombination Experiments (21[4]).

Statistical analysis

Statistical analyses were carried out using Dunnett's multiple-comparison test and the Tukey-Kramer test implemented in R (35). Significance was defined as a *p*-value of less than 0.05 (*$p < 0.05$, **$p < 0.01$, ***$p < 0.001$ or †$p < 0.05$, ††$p < 0.01$, ††† $p < 0.001$).

Table 2. Patch analysis in patch #1

Mutation	*dStability*[1]	Difference in patch area[2]			Number of patches		
		Hydrophobic	Positively charged	Negatively charged	Hydrophobic	Positively charged	Negatively charged
F235F	0	0	0	0	4	8	6
F235A	0.732571702	-100	0	0	3	8	6
F235R	1.006989541	-100	70	0	3	9	6
F235N	1.326652932	-90	0	40	3	8	7
F235D	1.350250176	-90	-10	80	3	8	8
F235C	0.939680112	-40	0	0	4	8	6
F235Q	0.900006362	-100	0	40	3	8	7
F235E	0.983574176	-90	0	80	3	8	7
F235G	0.505783926	-100	0	0	3	8	6
F235H	1.171110151	-100	0	80	3	8	7
F235I	0.25064059	-20	0	0	4	8	6
F235L	0.371927627	-10	0	0	4	8	6
F235K	1.080934474	-100	80	-40	3	9	6
F235M	0.431841099	-40	0	40	4	8	7
F235P	6.260009515	-90	0	40	3	8	7
F235S	0.956733005	-100	0	0	3	8	6
F235T	0.951938437	-90	0	40	3	8	7
F235W	0.781937796	-10	0	40	4	8	7
F235Y	0.78841556	-10	0	0	4	8	6
F235V	0.473775789	-30	0	40	4	8	7

[1] *dStability* (kcal/mol) is defined as the change in stability with no amino acid substitution as zero.
[2] The patch area (Å^2) of VP35 IID with the wildtype amino acid is zero, and the difference in patch area with each amino acid substitution is shown.

Table 3. Patch analysis in patch #2

Mutation	*dStability*[1]	Difference in patch area[2]			Number of patches		
		Hydrophobic	Positively charged	Negatively charged	Hydrophobic	Positively charged	Negatively charged
L232L	0	0	0	0	4	7	8
L232A	2.6275545	0	0	0	4	7	8
L232R	38.611566	-20	40	0	4	7	9
L232N	2.2629841	0	0	0	4	7	8
L232D	2.5580598	0	0	10	4	7	8
L232C	2.3945202	0	0	0	4	7	8
L232Q	2.0728772	0	0	0	4	7	8
L232E	2.0544426	0	0	0	4	7	8
L232G	3.6574852	0	0	0	4	7	8
L232H	2.8965719	0	0	-10	4	7	8
L232I	1.4270586	0	0	0	4	7	8
L232K	4.3843962	0	0	0	4	7	8
L232M	1.7285597	0	0	0	4	7	8
L232F	10.723272	20	0	0	4	7	8
L232P	29.928462	0	0	0	4	7	8
L232S	2.8143106	0	0	0	4	7	8
L232T	2.2331049	0	0	0	4	7	8
L232W	19.4083	20	0	0	4	7	8
L232Y	11.386522	-10	0	0	4	7	8
L232V	2.0320788	0	0	0	4	7	8
A238A	0	0	0	0	4	7	8
A238R	2.0994365	-70	40	0	3	7	9
A238N	0.9907217	-20	0	0	4	7	8
A238D	1.5951034	-10	0	60	4	8	8
A238C	0.8510315	0	0	0	4	7	8
A238Q	1.5488139	-70	0	0	3	7	8
A238E	2.7834175	-20	0	40	4	8	8
A238G	1.6270258	0	0	0	4	7	8
A238H	1.9547632	-20	0	60	4	8	8
A238I	5.7143486	-10	0	0	4	7	8
A238L	9.4618888	0	0	0	4	7	8
A238K	8.2175848	-20	50	0	4	7	8

A238M	1.5190067	-10	0	0	4	7	8
A238F	1.3228297	10	0	0	4	7	8
A238P	0.5634073	0	0	0	4	7	8
A238S	0.9860292	0	0	0	4	7	8
A238T	1.5008972	0	0	0	4	7	8
A238W	2.0445495	40	0	0	4	7	8
A238Y	1.1203081	-10	0	0	4	7	8
A238V	2.5027563	-10	0	0	4	7	8
F239F	0	0	0	0	4	7	8
F239A	1.9057251	-20	10	0	4	7	8
F239R	1.6876262	-80	60	0	3	7	9
F239N	1.8570417	-70	0	0	3	7	8
F239D	2.1112167	-80	0	0	3	7	8
F239C	1.8044742	-30	0	0	4	7	8
F239Q	1.3112751	-70	0	0	3	7	8
F239E	1.760937	-70	0	0	3	7	8
F239G	2.81543	-30	10	0	4	7	8
F239H	1.838075	-70	0	0	3	7	8
F239I	2.1238505	-10	0	0	4	7	8
F239L	0.7491947	-10	0	0	4	7	8
F239K	1.8976756	-70	60	0	3	7	9
F239M	1.3301483	-10	0	0	4	7	8
F239P	6.9946532	-10	0	0	4	7	8
F239S	2.1576557	-80	0	0	3	7	8
F239T	1.7906735	-30	0	0	4	7	8
F239W	1.4098491	10	0	0	4	7	8
F239Y	0.7401587	-70	0	0	3	7	8
F239V	1.8329102	0	0	0	4	7	8
Q274Q	0	0	0	0	3	7	8
Q274A	0.9790117	60	0	0	4	7	8
Q274R	0.6115132	50	60	0	4	7	9
Q274N	1.0520914	50	0	0	4	7	8
Q274D	1.3061332	50	0	0	4	7	8
Q274C	0.8424939	100	0	0	4	7	8
Q274E	1.0742681	60	0	0	4	7	8
Q274G	1.565205	70	10	0	4	7	8

Q274H	1.0874786	50	0	0	4	7	8
Q274I	0.824607	110	0	0	4	7	8
Q274L	0.1510161	120	0	0	4	7	8
Q274K	0.9377139	40	70	0	4	7	9
Q274M	0.3732078	110	0	0	4	7	8
Q274F	0.8585927	120	0	0	4	7	8
Q274P	56.740468	100	0	0	4	7	8
Q274S	1.2294898	50	0	0	4	7	8
Q274T	0.8657571	90	0	0	4	7	8
Q274W	0.9901868	140	0	0	4	7	8
Q274Y	1.2227983	120	0	0	4	7	8
Q274V	0.5805623	110	0	0	4	7	8
I278I	0	0	0	0	4	7	8
I278A	1.9591054	-10	40	0	4	7	8
I278R	1.3934811	-90	70	-10	3	7	9
I278N	1.9687262	-80	40	0	3	7	9
I278D	2.2570228	-80	0	60	3	8	8
I278C	1.9057499	-10	40	0	4	7	9
I278Q	1.6894351	-80	40	0	3	7	9
I278E	1.6783633	-80	0	40	3	8	8
I278G	2.752968	-30	10	0	4	7	8
I278H	1.9107519	-80	0	40	3	8	8
I278L	0.8558835	-10	0	0	4	7	8
I278K	1.5554021	-30	50	0	4	7	9
I278M	0.9461162	-30	0	0	4	7	8
I278F	1.1611346	-20	0	0	4	7	8
I278P	153.5848	-10	0	0	4	7	8
I278S	2.1471819	-80	40	0	3	7	9
I278T	1.6575709	-80	0	0	3	7	8
I278W	1.5097841	-10	0	-40	4	6	8
I278Y	1.2976086	-30	0	0	4	7	8
I278V	1.0096868	-10	0	0	4	7	8

[1] *dStability* (kcal/mol) is defined as the change in stability with no amino acid substitution as zero.

[2] The patch area (Å^2) of VP35 IID with the wildtype amino acid is zero, and the difference in patch area with each amino acid substitution is shown.

Table 4. Patch analysis in patch #3

Mutation	*dStability*[1]	Difference in patch area[2]			Number of patches		
		Hydrophobic	Positively charged	Negatively charged	Hydrophobic	Positively charged	Negatively charged
V245V	0	0	0	0	110	4	7
V245A	1.94009808	-10	0	0	4	7	8
V245R	1.73968582	-110	30	0	3	7	8
V245N	1.96042938	-10	0	0	4	7	8
V245D	2.16483607	-10	0	0	4	7	8
V245C	1.804856894	0	0	0	4	7	8
V245Q	2.52690014	0	0	0	4	7	8
V245E	4.685006891	-60	0	40	4	8	8
V245G	2.939590088	-10	0	0	4	7	8
V245H	10.29826373	-10	0	0	4	7	8
V245I	1.420383087	0	0	0	4	7	8
V245L	34.03914758	0	0	0	4	7	8
V245K	37.98844083	-110	0	0	3	7	8
V245M	2.76672884	0	0	0	4	7	8
V245F	825.8513853	-10	0	0	4	7	8
V245P	588.9697724	0	0	0	4	7	8
V245S	2.085385378	-10	0	0	4	7	8
V245T	2.209940464	-10	0	0	4	7	8
V245W	72.62961212	10	0	0	4	7	8
V245Y	95887186.48	-10	0	0	4	7	8
K248K	0	0	0	0	4	7	8
K248A	0.095168878	-10	-40	40	4	8	8
K248R	-0.519800474	-100	-30	40	3	8	8
K248N	0.28260355	-10	-50	40	4	8	8
K248D	0.6330468	-50	-40	70	4	8	8
K248C	0.085650141	-10	-40	40	4	8	8
K248Q	0.29007365	-10	-40	0	4	7	8
K248E	0.532215671	-10	-50	70	4	8	8
K248G	0.552775281	-10	-40	40	4	8	8
K248H	0.291377256	-10	-50	90	4	9	8
K248I	-0.68891395	40	-30	0	4	7	8
K248L	-0.640784223	30	-40	0	4	7	8

K248M	-0.248851966	10	-40	40	4	8	8
K248F	0.100037599	50	-40	0	4	7	8
K248P	981.5469749	-10	-40	40	4	8	8
K248S	0.242675293	-10	-40	40	4	8	8
K248T	0.006153339	-10	-40	0	4	7	8
K248W	-0.990039757	80	-20	40	5	8	8
K248Y	-0.814420669	20	-30	40	4	8	8
K248V	-0.391183967	20	-40	0	4	7	8
L249L	0	0	0	0	4	7	8
L249A	2.055125935	-20	0	0	4	7	8
L249R	1.255585451	-30	0	-10	4	7	8
L249N	1.910848759	-30	0	0	4	7	8
L249D	1.984240956	-50	0	40	4	8	8
L249C	1.941255393	0	0	0	4	7	8
L249Q	1.744715848	-40	0	-10	4	7	8
L249E	1.946672273	-40	0	30	4	7	8
L249G	2.884809407	-20	0	0	4	7	8
L249H	1.687257971	-30	0	30	4	7	8
L249I	1.278723454	0	0	0	4	7	8
L249K	1.786890975	-20	0	-10	4	7	8
L249M	1.29713662	-20	0	0	4	7	8
L249F	0.750303334	10	0	0	4	7	8
L249P	432.4197974	0	0	0	4	7	8
L249S	2.255533647	-50	0	0	4	7	8
L249T	2.204444709	-10	0	0	4	7	8
L249W	0.885336346	20	0	0	4	7	8
L249Y	0.834071571	0	0	0	4	7	8
L249V	1.628334062	0	0	0	4	7	8
A290A	0	0	0	0	4	7	8
A290R	0.504601777	-10	70	-30	4	7	9
A290N	0.723215064	-20	0	-10	4	7	8
A290D	1.120206587	-20	0	50	4	7	8
A290C	0.796192933	0	0	-10	4	7	8
A290Q	0.86041541	-20	0	20	4	7	8
A290E	0.987338204	-20	0	50	4	7	8
A290G	1.482704634	0	0	0	4	7	8

A290H	1.361392088	-20	0	40	4	7	8
A290I	5.390960481	20	0	-10	4	7	8
A290L	-0.123682767	20	10	-10	4	7	8
A290K	1.037420222	-30	70	-10	4	7	9
A290M	0.526912091	20	0	0	4	7	8
A290F	0.542257567	40	0	-10	4	7	8
A290P	1125.794701	0	0	-10	4	7	8
A290S	1.023275747	-20	0	-10	4	7	8
A290T	0.941858651	-10	0	0	4	7	8
A290W	1.004867449	60	0	-10	4	7	8
A290Y	0.616011644	20	10	-10	4	7	8
A290V	3.577328926	0	0	-10	4	7	8
P293P	0	0	0	0	4	7	8
P293A	1.067504566	-10	0	0	4	7	8
P293R	0.133816822	-110	40	0	3	7	8
P293N	1.035976962	-110	0	0	3	7	8
P293D	1.328013011	-110	0	0	3	7	8
P293C	1.023459389	-10	0	0	4	7	8
P293Q	0.68896101	-110	0	0	3	7	8
P293E	0.707244618	-110	-10	0	3	7	8
P293G	1.856066142	-30	0	0	4	7	8
P293H	1.538806997	-20	-10	0	4	7	8
P293I	0.019388362	0	0	0	4	7	8
P293L	-0.054958234	10	0	0	4	7	8
P293K	1.052286242	-50	50	0	4	7	8
P293M	0.207329841	0	0	0	4	7	8
P293F	0.85928369	60	0	0	4	7	8
P293S	1.262504563	-110	0	0	3	7	8
P293T	0.758316384	-60	0	0	4	7	8
P293W	0.894564793	20	0	0	4	7	8
P293Y	0.963431749	30	0	0	4	7	8
P293V	0.022220093	0	0	0	4	7	8
I295I	0	0	0	0	4	7	8
I295A	2.023302934	-10	0	-40	4	6	8
I295R	0.859431366	-110	10	0	3	7	8
I295N	1.99553434	-50	0	0	4	7	8

I295D	2.253890578	-60	0	60	4	8	8
I295C	2.039158126	-40	0	-40	4	6	8
I295Q	1.479317877	-50	0	0	4	7	8
I295E	1.916342451	-50	0	40	4	8	8
I295G	2.763974997	-20	0	-40	4	6	8
I295H	1.957786738	-50	0	50	4	8	8
I295L	0.751394736	0	0	0	4	7	8
I295K	1.623988688	-50	40	0	4	7	9
I295M	1.176933426	-10	0	0	4	7	8
I295F	0.704692173	0	0	0	4	7	8
I295P	82.9752419	-10	0	0	4	7	8
I295S	2.240752554	-40	0	0	4	7	8
I295T	1.789046233	-50	0	0	4	7	8
I295W	0.879898913	0	0	0	4	7	8
I295Y	0.974483428	-10	0	0	4	7	8
I295V	1.08541018	-10	0	0	4	7	8
I297I	0	0	0	0	4	7	8
I297A	2.217895682	-10	0	-40	4	6	8
I297R	2.275249985	-30	0	0	4	7	8
I297N	2.026114101	-10	0	0	4	7	8
I297D	2.536684628	-10	0	-40	4	6	8
I297C	2.030322076	-10	0	-40	4	6	8
I297Q	2.05753488	-20	0	0	4	7	8
I297E	2.390634188	-20	0	80	4	8	8
I297G	3.133241422	-10	10	-40	4	6	8
I297H	2.838109053	-20	0	70	4	8	8
I297L	1.592453204	0	0	0	4	7	8
I297K	2.991622117	-30	0	0	4	7	8
I297M	1.846678482	-10	0	0	4	7	8
I297F	2.136438321	10	0	0	4	7	8
I297P	23.19278575	-10	0	-40	4	6	8
I297S	2.408419279	-10	0	-40	4	6	8
I297T	1.925662195	-10	0	-40	4	6	8
I297W	3.220605793	40	0	-40	4	6	8
I297Y	1.83253497	0	0	0	4	7	8
I297V	1.132516364	-10	0	0	4	7	8

F328F	0	0	0	0	4	7	8
F328A	2.983770293	30	0	0	4	7	8
F328R	1.92821213	-20	0	0	4	7	8
F328N	2.841497587	-10	0	0	4	7	8
F328D	2.925697332	-10	0	0	4	7	8
F328C	2.868945471	20	0	0	4	7	8
F328Q	2.543589049	0	0	0	4	7	8
F328E	2.859739658	-20	0	0	4	7	8
F328G	3.985298561	40	0	-40	4	6	8
F328H	2.421494646	-10	0	0	4	7	8
F328I	22.58227036	10	0	0	4	7	8
F328L	1.980802214	0	0	0	4	7	8
F328K	2.331466483	-20	0	0	4	7	8
F328M	1.87006816	-10	0	0	4	7	8
F328P	119.9410066	30	0	0	4	7	8
F328S	3.206147808	0	0	0	4	7	8
F328T	2.506706817	20	0	0	4	7	8
F328W	1.162626502	0	0	0	4	7	8
F328Y	0.941289061	0	0	0	4	7	8
F328V	2.672337747	20	0	0	4	7	8

[1] *dStability* (kcal/mol) is defined as the change in stability with no amino acid substitution as zero.
[2] The patch area ($Å^2$) of VP35 IID with the wildtype amino acid is zero, and the difference in patch area with each amino acid substitution is shown.

Table 5. Patch properties and effects of amino acid substitutions

Patch	Mutation	*dStability*[1]	Difference in patch area[2]			Number of patches		
			Hydrophobic	Positively charged	Negatively charged	Hydrophobic	Positively charged	Negatively charged
#1	F235F	0.00	0	0	0	3	8	6
	F235A[3]	0.73	-100	0	0	2	8	6
	F235G[3]	0.51	-100	0	0	2	8	6
	F235S[3]	0.96	-100	0	0	2	8	6
	F235L[4]	0.37	-10	0	0	3	8	6
	F235Y[4]	0.79	-10	0	0	3	8	6
#2	A238A	0.00	0	0	0	3	8	6
	A238Q[3]	1.55	-70	0	0	2	8	6
	A238P[4]	0.56	0	0	0	3	8	6
	F239F	0.00	0	0	0	3	8	6
	F239Q[3]	1.31	-70	0	0	2	8	6
	F239N[3]	1.86	-70	0	0	2	8	6
	F239H[3]	1.84	-70	0	0	2	8	6
	F239K[3]	1.90	-70	60	0	2	9	6
	F239A[3]	1.91	-20	10	0	2	8	6
	F239Y[3]	0.74	-70	0	0	2	8	6
	F239V[4]	1.83	0	0	0	3	8	6
	I278I	0.00	0	0	0	3	8	6
	I278T[3]	1.66	-80	0	0	2	8	6
#3	P293P	0.00	0	0	0	3	8	6
	P293N[3]	1.04	-110	0	0	2	8	6
	P293D[3]	1.33	-110	0	0	2	8	6
	P293Q[3]	0.69	-110	0	0	2	8	6
	P293S[3]	1.26	-110	0	0	2	8	6
	P293I[4]	0.02	0	0	0	3	8	6
	I295L[4]	0.75	0	0	0	3	8	6

[1] *dStability* (kcal/mol) is defined as the change in stability with no amino acid substitution as zero.
[2] The patch area (Å^2) of VP35 IID with the wildtype amino acid is zero, and the difference in patch area with each amino acid substitution is shown.
[3] Mutations that were used as patch-disrupted mutants in this study (shown in boldface).
[4] Mutations that were used as the mutants that retained the properties of the patch in this study.

Results

Hydrophobic patches present on the surface of VP35 IID and amino acid substitutions to modify the patch properties

To test the hypothesis that hydrophobic regions of IID are important for the polymerase cofactor function and IFN-antagonist activity of VP35, I first aimed to identify hydrophobic regions (i.e., hydrophobic patches) on the surface of EBOV VP35 IID. Using *in silico* analysis, I found three regions that had hydrophobic properties on the IID surface (Figure 7A). These hydrophobic patches consisted of multiple amino acid residues: Patch #1 consisting of F235, patch #2 consisting of L232, A238, F239, Q274, and I278, and patch #3 consisting of V245, K248, L249, A290, P293, I295, I297, and F328. Some of these amino acid residues were located in the hydrophobic region that has been previously described (22, 52, 62). Particularly, F239 has been previously described as an essential amino acid that is important for dsRNA binding and suppression of the IFN-β promoter activation, and K248 belonging to the basic patch has been shown to be responsible for the VP35-NP interaction (21, 52). I then compared corresponding amino acid residues among filoviruses (Figure 7B). Most of the amino acids comprising the hydrophobic patches were shared among ebolaviruses but only partially with LLOV, MLAV, and MARV. Consistent with a previous study (52), it was noted that several amino acids such as F239 and P293 were conserved among all filoviruses (Figure 7B). I hypothesized that these hydrophobic patches might act as functional sites of VP35 and investigated the biological importance of each amino acid residue in the following experiments. For this purpose, I first sought amino acid substitutions that had little effect on the overall stability of the VP35 IID but eliminated the hydrophobic patches. For each amino acid that constituted the hydrophobic patches, the area size of the patch, the effect on other patches, and the stability of the patch were calculated when substituted for by 19 other amino acids *in silico*. I identified 15 substitutions at 5 positions (235, 238, 239, 278, and 293) (Table 5). Then plasmids for the expression of wildtype VP35, the previously known dysfunctional VP35 R225E mutant (21), and 15 VP35 mutants with the identified substitutions were constructed.

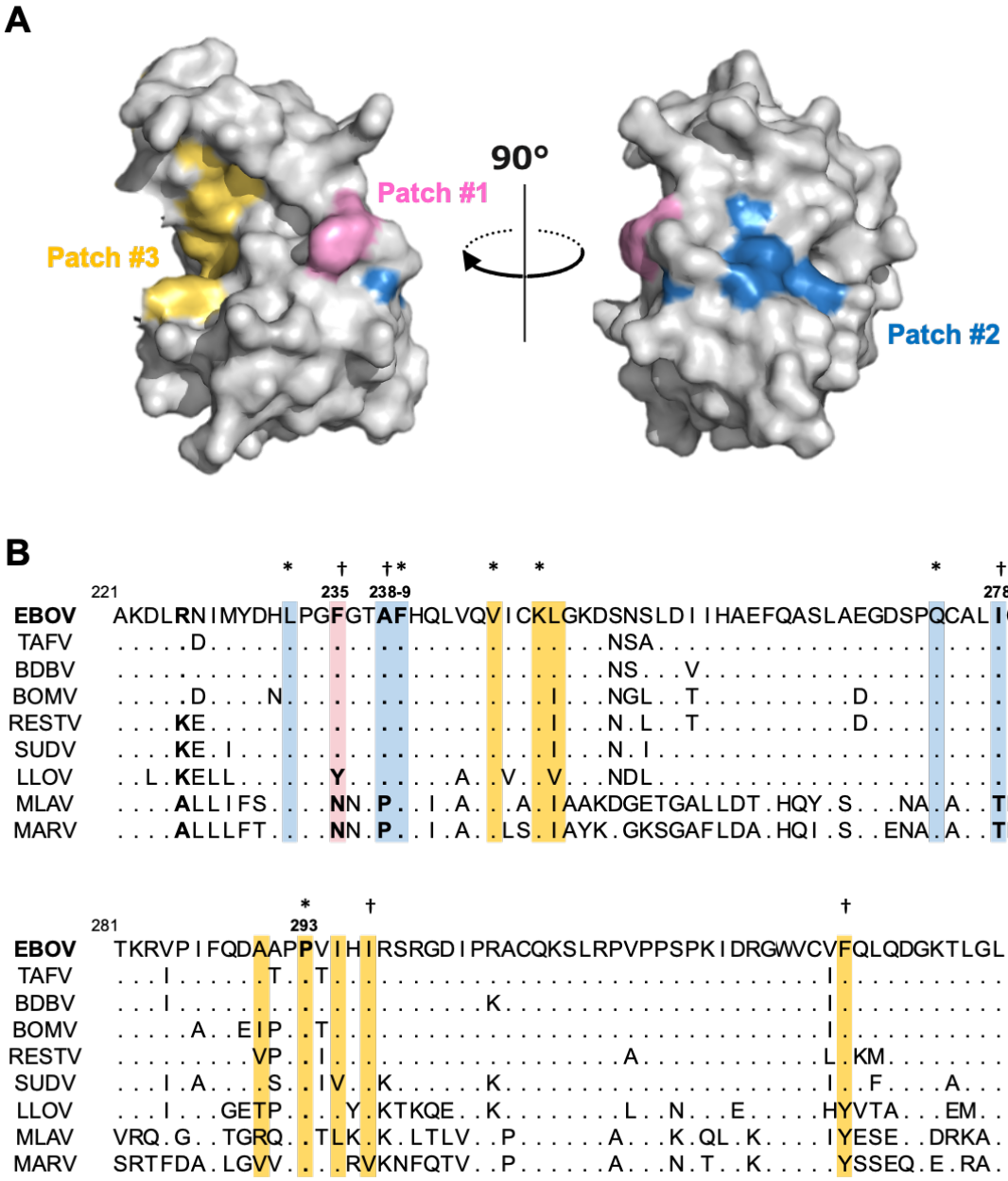

Figure 7. Hydrophobic patches on the VP35 IID surface

(A) Three hydrophobic patches are shown on a structural model of VP35 IID (PDB ID: 3FKE). Patch #1 contains a single residue F235 (red). Patch #2 contains residues L232, A238, F239, Q274, and I278 (blue). Patch #3 contains residues V245, K248, L249, A290, P293, I295, I297, and F328 (yellow). (B) Multiple amino acid sequence alignment of VP35 IID among filovirus species. Highlighted amino acids represent those involved in the respective hydrophobic patches (red: patch #1, blue: #2, yellow: #3). Amino acids that are conserved among filoviruses and ebolaviruses are indicated by asterisks and daggers, respectively.

Reduced function as a polymerase cofactor in patch-disrupted VP35 mutants

Since VP35 is required for EBOV genome replication as a viral polymerase cofactor (21, 63, 64), the modification of VP35 might affect polymerase activity. To investigate the functionality of VP35 for the EBOV genome transcription and replication, a plasmid-based EBOV minigenome assay was used (60). HEK293T cells were cotransfected with the EBOV minigenome plasmid encoding the firefly luciferase and expression plasmids encoding the T7 RNA polymerase, EBOV L, NP, VP30, and VP35. The luciferase activity in the cell lysate was then analyzed (Figure 8A). The expression of the luciferase from the EBOV minigenome was significantly impaired by F239K substitution in patch #2 and all of the substitutions tested in patch #3 (positions 293), but no significant difference in the VP35 expression in the transfected cells was observed in immunoblotting. On the other hand, none of the substitutions in patch #1 significantly altered the luciferase expression compared to that in the presence of wildtype VP35. These results suggested that disruption of hydrophobic patch #2 and patch #3 decreased viral replication and that the hydrophobic regions of IID were important for the polymerase cofactor activity of VP35. The subcellular localization of the representative VP35 mutants in plasmid-transfected HEK293T cells was found to be similar to that of the wildtype in immunofluorescence assays (Figure 9).

To confirm the importance of the hydrophobic properties of patches #2 and #3 for the polymerase cofactor function, I tested VP35 mutants having amino acid substitutions that did not impair the hydrophobic patches and had little effect on the protein structure in the patch analysis (Table 5 and Figure 8B). As expected, none of the amino acid substitutions in patch #1 (F235L and F235Y) significantly reduced the luciferase activity compared to the F235G mutant. In contrast, the mutants that retained the properties of patch #2 (A238P and F239V) showed higher polymerase cofactor activity than the patch-disrupted mutants (A238Q and F239K, respectively). For two patch-retained mutants of patch #3 (I295L and P293I), there was no significant difference in polymerase cofactor activities compared to those of the patch-disrupted mutants (P293N and P293S), suggesting that disruption of the hydrophobic property of patch #3 was not the principal determinant for the reduction of the polymerase cofactor function of VP35. These results suggested that the hydrophobic property of patch #2 on VP35 IID was important for the polymerase cofactor function of VP35.

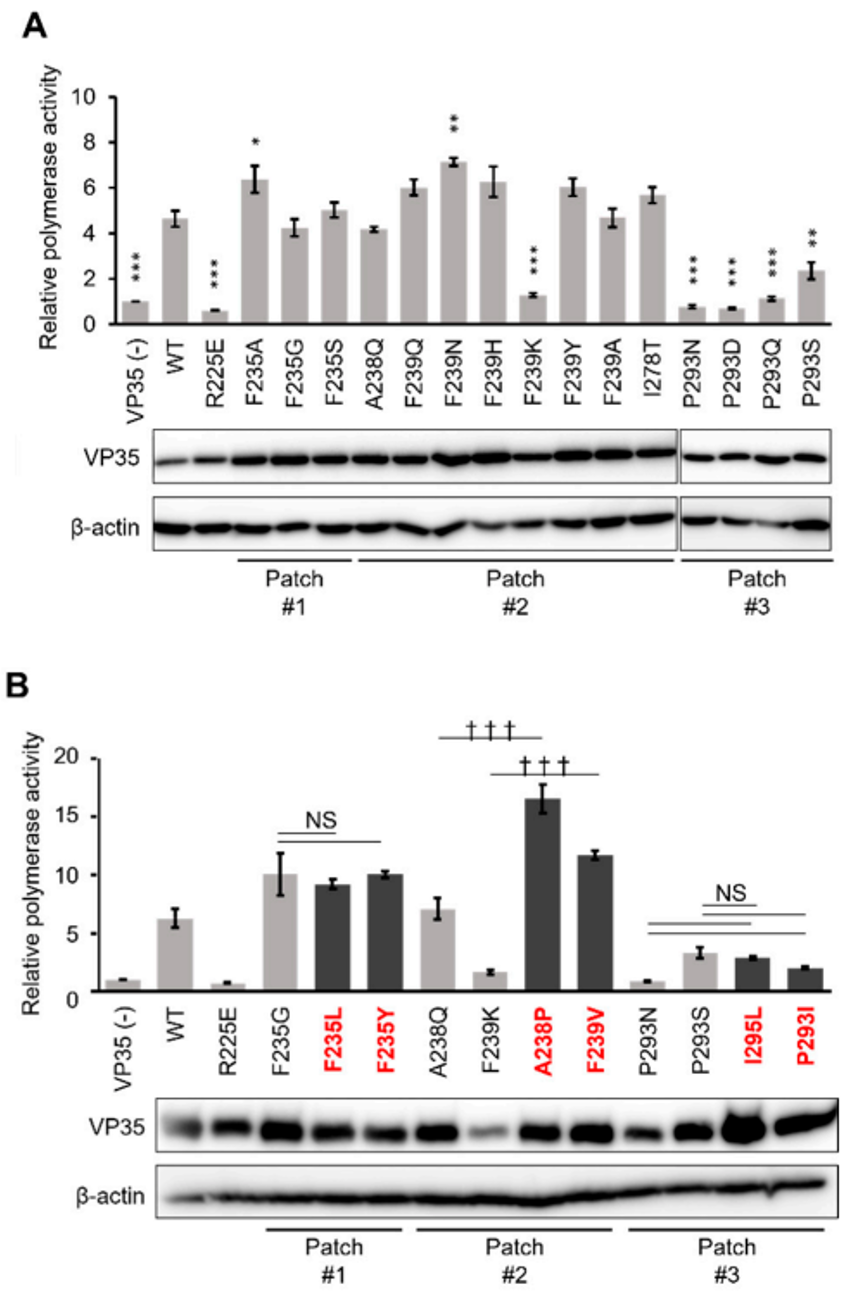

Figure 8. Attenuation of polymerase cofactor activity of hydrophobic patch-disrupted mutants of VP35.

Viral polymerase activity was assessed by minigenome assay. HEK293T cells were transfected with an empty vector (VP35(-)), WT-, or mutant VP35-expressing plasmids together with expression plasmids for EBOV NP, VP30, L, T7 RNA polymerase, and a plasmid providing the EBOV minigenome encoding a fused firefly luciferase reporter gene under the control of the T7 RNA polymerase promoter. A Renilla luciferase-expression plasmid was cotransfected as a control for transfection efficiency.

Minigenome activity was quantified by measuring firefly luciferase activity, and this was normalized to the level of Renilla luciferase expression. Each patch-disrupted mutant was analyzed to compare with wildtype VP35 (A) and patch-retained mutants (B). Each bar represents mean ± SE for three independent experiments. Lower panels show western blots for VP35 proteins. Mutants shown in red boldface (also shown with dark bars) are those that retained the hydrophobic patch. Dunnett's multiple-comparison test was used for the comparison to wildtype (WT) (*$p < 0.05$, **$p < 0.01$, ***$p < 0.001$)(A). The Tukey-Kramer test was used for comparisons between the patch-disrupted and patch-retained mutants in each amino acid position (†$p < 0.05$, ††$p < 0.01$, †††$p < 0.001$, NS: No significant difference)(B).

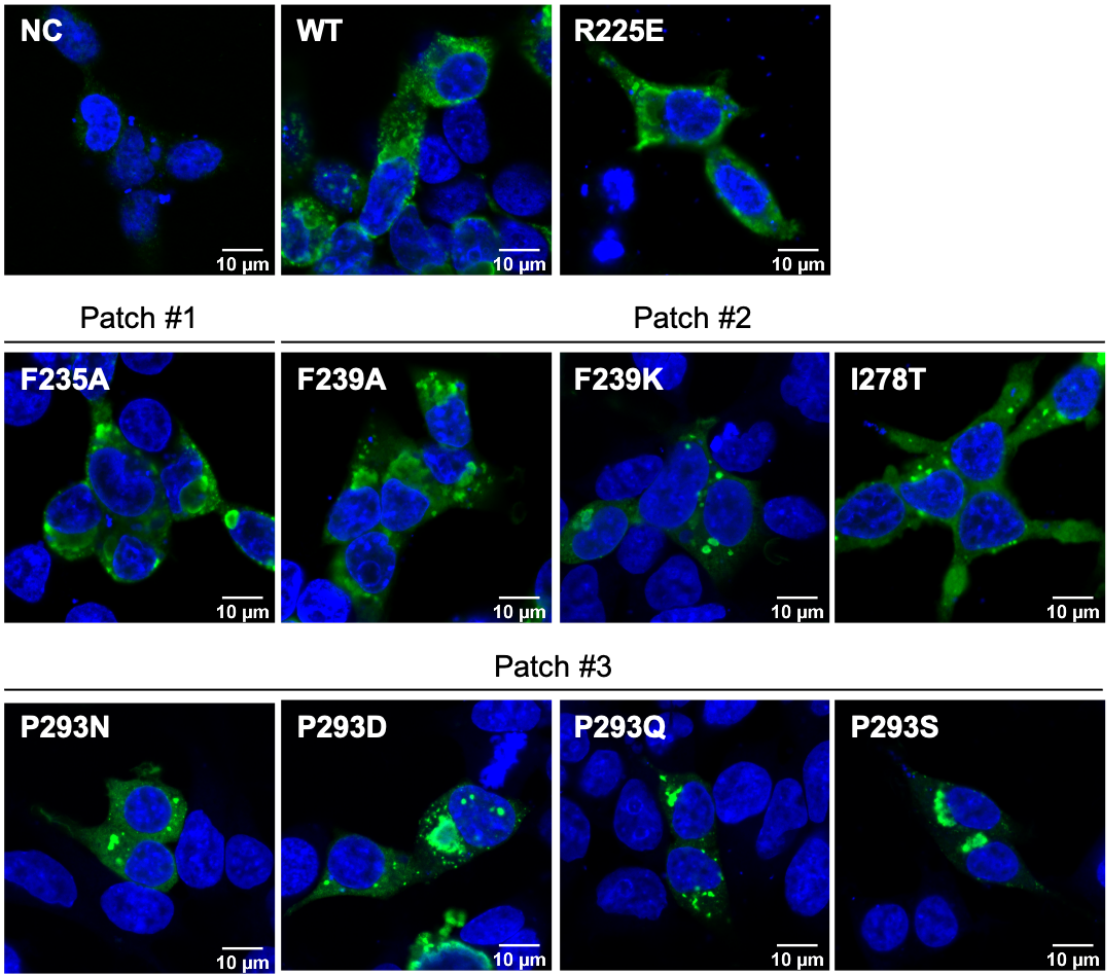

Figure 9. Subcellular localization of VP35 mutants

Subcellular localization of VP35 was confirmed by immunofluorescence analysis. HEK293T cells were transfected with an empty vector, WT, or mutant VP35-expressing plasmids. HA-tagged WT or VP35 mutants were detected with a monoclonal anti-HA antibody (Abcam) and Alexa488-labeled anti-mouse IgG (H+L)(Life Technologies). DAPI (blue) was used for nuclear staining.

Reduced interaction between NP and patch-disrupted VP35 mutants having lower polymerase cofactor activity

The interaction between VP35 and NP is essential for EBOV polymerase activity. Previously, IID was shown to be sufficient for the interaction with NP. It was also shown that amino acid residues in one of the basic patches, consisting of residues K222, R225, K248, and K251, was critical for both polymerase cofactor function and the interaction with NP (21, 52). To determine whether the modification of the hydrophobic patches could affect the VP35-NP interaction, VP35 (wildtype and mutants) and NP were expressed in HEK293T cells and their interactions were analyzed by immunoprecipitation assays (Figure 10A and B). I first selected the most stable patch-disrupted mutants (i.e., those with the lowest *dStabilities* predicted by the patch analysis shown in Table 5) in each amino acid position (F235G for #1 and #2: A238Q, F239Y, and I278T for #2, and P293Q for #3) predicted by the patch analysis (Table 5) for this experiment. It was found that the interaction between VP35 and NP was significantly weakened by the P293Q substitution in patch #3 but not by the mutations in patch #1 and #2. To confirm the importance of patch #3 in the VP35-NP interaction, the other patch #3 mutants were also tested in immunoprecipitation assays (Figure 10C). I found that the amounts of NP immunoprecipitated with these patch #3 mutants were at almost undetectable levels although the band intensities of immunoprecipitated patch #3 VP35 mutants were weaker than that of wildtype VP35. I also tested the patch #2 F239K mutant, which showed low polymerase cofactor activity, and found that NP was not immunoprecipitated (Figure 10D). However, since the mutant was less effectively immunoprecipitated than wildtype VP35, it was not clarified whether the low polymerase cofactor activity was due to reduced interaction between NP and the F239K mutant. It is conceivable that the substitution might cause decreased solubility and stability of the protein, resulting in reduced immunoprecipitation efficiency.

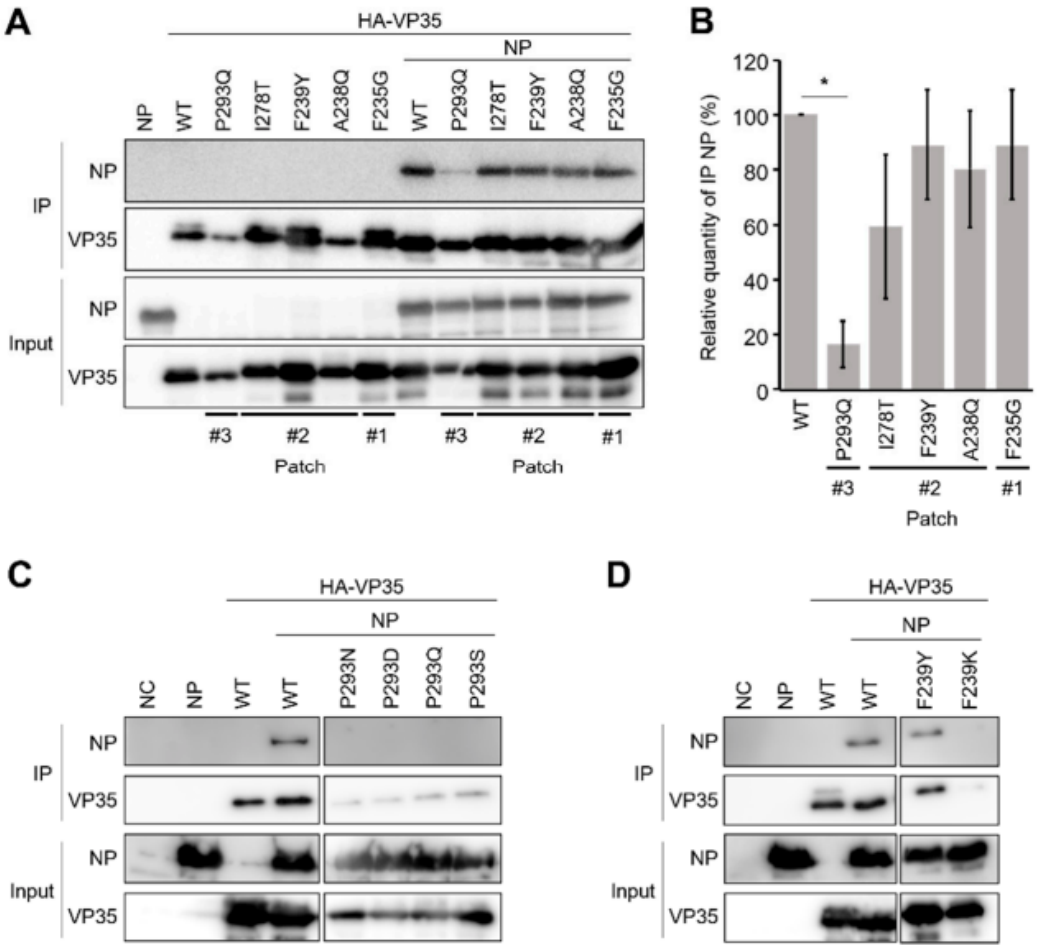

Figure 10. NP-VP35 interaction attenuated by hydrophobic patch modifications in VP35 IID. (A, C, and D) Representative western blot images of EBOV NP immunoprecipitated from HEK293T cells transfected with the plasmids expressing EBOV NP and with wildtype VP35 (WT) or VP35 mutants. Representative mutants for patches #1, #2, and #3 (A), patch #3-disrupted mutants (B), and F239 mutants (patch #2) (C) were analyzed. Cells were lysed with a lysate buffer 36 hours post-transfection. Then NP-bound HA-tagged VP35 was precipitated from samples using anti-HA affinity gel beads and analyzed by western blotting. (B) Band intensities of immunoprecipitated NP relative to VP35 are quantified by western blotting. Each bar represents mean ± SE from three independent experiments. Dunnett's multiple-comparison test was used to compare to WT (*$p < 0.05$).

Decreased IFN antagonism of patch-disrupted VP35 mutants

VP35 inhibits the RIG-I pathway for IFN production at multiple steps. For example, it acts as a suppressor of the cellular kinases IKKε and TBK1 (47, 50). The VP35 IID is thought to be required for suppression of IFN-α/β gene expression (53). Thus, I next analyzed the effect of the patch modification on the inhibitory activity of VP35 with regard to IFN-β activation. HEK293 cells were cotransfected with the reporter plasmids carrying the IFN-β promoter and luciferase genes, and the expression plasmids for VP35 and Renilla luciferase. Then IFN production was induced by poly(I:C) stimulation and IFN-β promoter activity was determined by a reporter assay (Figure 11). As previously reported, wildtype VP35 inhibited IFN-β promoter activation. Consistent with the previous finding (52), I found that the patch #1 mutants showed the same level of suppression of the IFN-β promoter activity as wildtype VP35 even though the expression levels of the mutants were almost the same as or lower than that of wildtype VP35. On the other hand, the patch #2 and #3 mutants showed little effect on the reduction of IFN-β promoter activity compared to wildtype VP35, although the expression levels of the mutants were almost the same as or lower than that of wildtype VP35, except for the F239Y mutant. Interestingly, some patch #2 mutants (A238Q, F239Q, F239N, and F239A) that did not affect the polymerase cofactor activity reduced the ability to suppress the IFN-β promoter activity (Figure 11A). The same experiment was carried out with the mutants that were predicted to have less significant changes in their patch properties (Figure 11B). Unexpectedly, there were no significant differences between the patch-disrupted mutants and the patch-retained mutants, except for A238P. The IFN-β promoter activity was significantly reduced by one of the patch #2 mutants (A238P), which was comparable to wildtype VP35. Since the expression level of the A238P mutant was higher than those of the other patch #2 mutants, it could not be ruled out that the strong inhibition of IFN-β promoter activity by A238P might have been due to this difference. However, the expression levels of VP35 did not generally correlate with the suppression of IFN-β promoter activity. These findings suggested that amino acid residues in patches #2 and #3 of VP35 were important for the suppression of IFN production although the patch hydrophobicity was not the only factor for the functional importance.

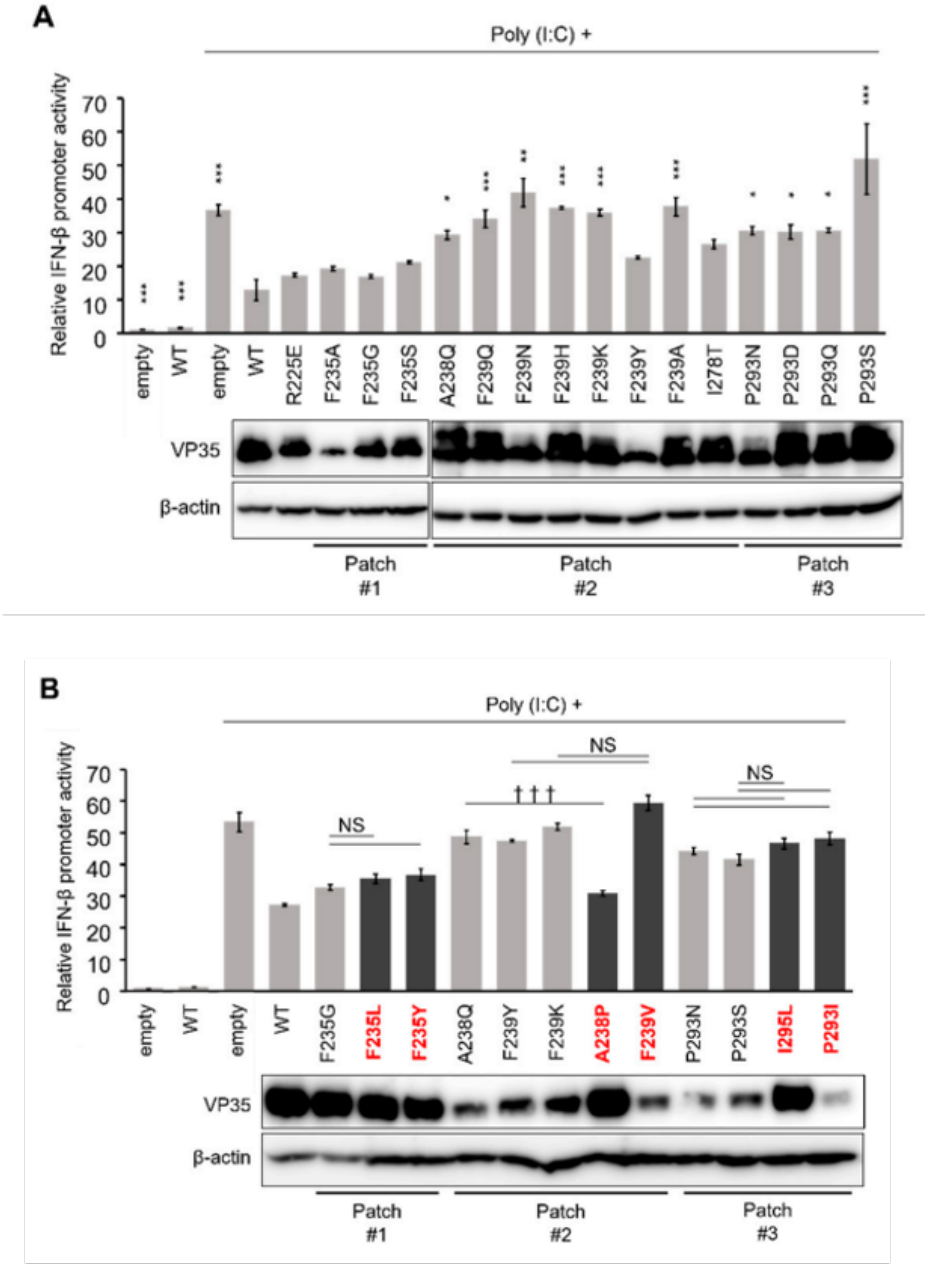

Figure 11. Attenuation of polymerase cofactor activity of hydrophobic patch-disrupted mutants of VP35.

Viral polymerase activity was assessed by minigenome assay. HEK293T cells were transfected with an empty vector (VP35(-)), WT-, or mutant VP35-expressing plasmids together with expression plasmids for EBOV NP, VP30, L, T7 RNA polymerase, and a plasmid providing the EBOV minigenome encoding a fused firefly luciferase reporter gene under the control of the T7 RNA polymerase promoter. A Renilla luciferase-expression plasmid was cotransfected as a control for transfection efficiency. Minigenome activity was quantified by measuring firefly luciferase activity, and this was

normalized to the level of Renilla luciferase expression. Each patch-disrupted mutant was analyzed to compare with wild-type VP35 (A) and patch-retained mutants (B). Each bar represents mean ±SE for three independent experiments. Lower panels show Western blots for VP35 proteins and β-actin. Mutants shown in red boldface (also shown with dark bars) are those that retained the hydrophobic patch. Dunnett's multiple-comparison test was used for the comparison to WT (*$p < 0.05$, **$p < 0.01$, ***$p < 0.001$) (A). The Tukey–Kramer test was used for comparisons between the patch-disrupted and patch-retained mutants in each amino acid position (†††$p < 0.001$, NS: No significant difference) (B).

Discussion

Previous studies have provided insights into the structure and biological activity of EBOV VP35, which functions as a virulence factor that suppresses innate immunity and as a polymerase cofactor that is essential for viral RNA replication/transcription (21, 22, 54, 62). Although it has been shown that the VP35 function as a part of the viral polymerase complex appears to require its interaction with viral NP and L (18, 64) and that the C-terminal IID of VP35 is essential for both interaction with NP and antagonism of IFN production (21). The present study focused on the hydrophobic patches present on the surface of VP35 IID and further characterized the properties of the domain using an *in silico* analysis followed by site-directed mutagenesis in biological assays (Table 6).

The hydrophobic patches identified in the present study are partly overlapped with the functional region described previously in the hydrophobic pocket end cap and the first basic patch and some amino acid residues important for the VP35 functions have been identified in the previous studies (21, 52). Amino acid residues F235 and F239 on VP35 IID, which were predicted to form hydrophobic patches in my patch analysis, have been previously found to be functional amino acids by using alanine scanning mutagenesis (21, 52). The F235A substitution, but not F239A, was previously demonstrated to lose the function as a polymerase cofactor (52). However, in my experiments, while the F239A mutant retained the same level of polymerase cofactor function as wildtype VP35, the F235A mutant did not show significant loss of polymerase cofactor activity, inconsistent with previous reports. (Figure 8A). The discrepancy may be due to the difference in experimental conditions, sensitivity, and/or evaluation methods. However, considering that both F235A and F239A mutants were shown to retain the ability to bind to NP (21, 52), I assume that the F235A mutant does not completely lose its polymerase cofactor activity. In this study, the effects of F235A and F239A substitutions on IFN antagonism were similar to those found in a previous study (52); the F235A mutant had the ability to suppress IFN production as well as wildtype VP35, whereas the F239A mutant had reduced ability to suppress IFN production. These data suggest that my *in silico* patch analysis may be a useful tool to identify functional amino acids on molecular surfaces of proteins.

Although alanine scanning mutagenesis has been generally used to identify amino acid residues critical for protein functions, it was indeed unclear whether mutations to alanine fully altered the functions of the relevant proteins and whether each alanine mutation affected the overall stability of molecules. In this study, therefore, *in silico* analysis was performed to predict which amino acid residues could be used for substitutions that would disrupt each hydrophobic patch but not affect the protein

structure. In patch #2, among the mutations at position 239, only the F239K mutation greatly reduced the polymerase cofactor activity. This finding suggests an important role of the hydrophobicity in this VP35 function whereas it might also be possible that other factors such as the difference in the properties of these amino acid residues caused a structural change that might disrupt the polymerase cofactor function. As mentioned above, both in a previous report and in the present study, the F239A mutant showed polymerase cofactor activity comparable to that of wildtype VP35. This suggests that mutations to alanine are not necessarily sufficient to fully affect protein functions, and that substitutions to other amino acids should be considered for mutagenesis studies. On the other hand, it should also be noted that some amino acid substitutions may alter protein oligomerization or stability status, which potentially affect expression levels of proteins. This might be one of the reasons for inconsistent VP35 band intensities seen in this study.

In this study, I have shown for the first time that P293 of VP35 contributes to polymerase cofactor activity and IFN-β suppression. Using computer analyses, the P293 residue has been predicted to be important for the interaction with small molecule compounds that may potentially inhibit VP35 functions (65–67). However, the actual importance of this amino acid residue had not been evaluated in biological assays in vitro. In this study, I provide direct evidence that P293 is important for both polymerase cofactor function and suppression of IFN production, supporting the previous *in silico* studies that predicted the functional importance of this amino acid position (65–67). Interestingly, the VP35 functions were impaired even by the P293 mutants with amino acid substitutions that had little effect on the patch #3 hydrophobicity (Figure 8). This suggests that the unique properties of the proline residue at this position, as well as the hydrophobic feature of patch #3, are also important for VP35 functions.

In addition to the direct interaction with dsRNA, VP35 suppresses IFN production by interacting with TBK1 and IKKε and inhibiting post-translational modifications of IRF-3/7 (46). In this study, I was not able to clarify the detailed mechanisms by which the hydrophobic patches contribute to the suppression of IFN production. It has been reported that F239 and I278 interact with dsRNA in a van der Waals manner (52, 68), suggesting that the loss of patch #2 results in a decrease in the IFN-inhibitory capacity due to decreased binding to dsRNA. On the other hand, patch #3 is located far from the interaction site of dsRNA, suggesting that the contribution of patch #3 to the suppression of IFN production may be owing to other mechanisms (Figure 12).

Previous reports have shown that MARV, LLOV, and MLAV VP35s, as well as EBOV VP35, are involved in the suppression of IRF3 activation and IFN-I production

(46, 69, 70). MARV VP35 also binds to dsRNA, but it recognizes a longer nucleotide length than EBOV VP35: EBOV and MARV VP35s bind to 8 bp and 18 bp of dsRNA, respectively (68). Amino acid F239 (patch #2), which was found to affect the VP35 functions by point mutations (Figures 2 and 4), has been reported to be important for hydrophobic interactions with dsRNA (52, 68). However, since F239 is highly conserved among filoviruses (Figure 7), this residue may not mainly contribute to the difference in the RNA length of dsRNA recognition between EBOV and MARV. On other hand, amino acid P293 (patch #3), which is also conserved among filoviruses and important for the VP35 functions, is located far from the dsRNA recognition site (Figure 11). The common roles of P293 in IFN antagonisms among VP35s of filoviruses need to be clarified in future studies.

Although the development of therapeutic agents for Ebola virus disease is highly desirable, drug screening using infectious filoviruses such as EBOV can only be performed in biosafety level-4 facilities. For this reason, there are many computational attempts to create viral protein-specific inhibitors against EBOV by screening more than several million compounds *in silico*. Inhibitors against EBOV VP35 have also been screened based on structural information (52). My approach will help to establish a research basis for the development of filovirus therapeutics by linking computational analyses and biological experiments that do not need to use infectious viruses.

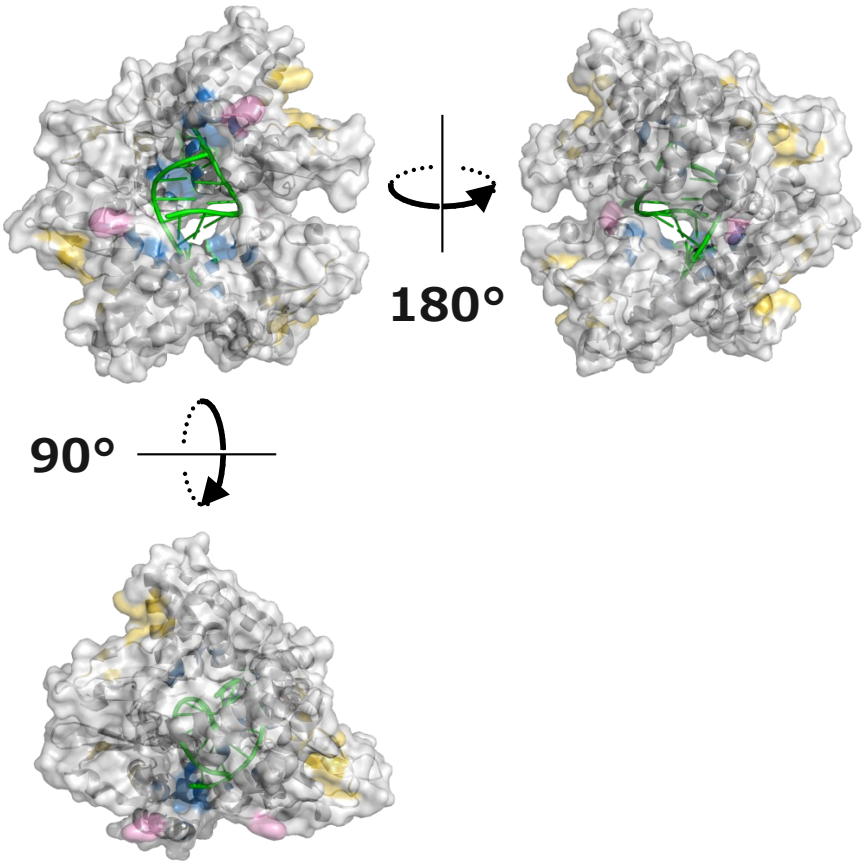

Figure 12. Structure of the VP35 IID-dsRNA complex.
Three-dimensional structures of the VP35 IID 401 tetramer complexed with dsRNA are shown (PDB ID: 3L26). The crystallographic asymmetric unit 402 contains four VP35 IID molecules and one 8 base-pair dsRNA (green). Hydrophobic patch regions 403 #1, #2, and #3 are shown in pink, blue, and yellow, respectively.

Table 6. Summary of patch analysis, minigenome replication, NP-interaction, and IFN-β promoter-suppression data

Hydrophobic patch	Effect on patch	VP35	Minigenome replication	Interaction with NP	Suppression of IFN-β promoter
#1	Disrupted	Wildtype	++	+	+++
		R225E	-	ND[1]	+++
		F235A	+++	ND	+++
		F235G	++	+	+++
		F235S	++	ND	+++
	Retained[2]	**F235L**	++	ND	+++
		F235Y	++	ND	+++
#2	Disrupted	A238Q	++	+	±
	Retained	**A238P**	+++	ND	+++
	Disrupted	F239Q	++	ND	-
		F239N	+++	ND	-
		F239H	++	ND	-
		F239K	-	-	-
		F239Y	++	+	+++
		F239A	++	ND	-
	Retained	**F239V**	++	ND	-
	Disrupted	I278T	++	ND	+++
#3	Disrupted	P293N	-	-	±
		P293D	-	-	±
		P293Q	-	-	±
		P293S	±	-	-
	Retained	**P293I**	-	ND	-
		I295L	±	ND	-

[1]ND: Not done

[2]Patch-retained mutants are shown in boldface.

Summary

VP35 of EBOV is a multifunctional protein that mainly acts as a viral polymerase cofactor and an interferon antagonist. VP35 interacts with NP and double-stranded RNA for viral RNA transcription/replication and inhibition of IFN-I production, respectively. The C-terminal portion of VP35, which is termed the IID, is important for both functions. To further identify critical regions in this domain, I analyzed the physical properties of the surface of VP35 IID, focusing on hydrophobic patches, which are expected to be functional sites that are involved in interactions with other molecules. Based on the known structural information of VP35 IID, three hydrophobic patches were identified on its surface and their biological importance was investigated using minigenome and IFN-β promoter-reporter assays. Site-directed mutagenesis revealed that some of the amino acid substitutions that were predicted to disrupt the hydrophobicity of the patches significantly decreased the efficiency of viral genome replication/transcription due to reduced interaction with NP, suggesting that the hydrophobic patches might be critical for the formation of a replication complex through the interaction with NP. It was also found that the hydrophobic patches were involved in the IFN-inhibitory function of VP35. These results high-light the importance of hydrophobic patches on the surface of EBOV VP35 IID and also indicate that patch analysis is useful for the identification of amino acid residues that directly contribute to protein functions.

Conclusion

In viral infections, both host and viral protein factors are involved in molecular mechanisms that cause detrimental reactions in a host animal. A single amino acid substitution in host and/or viral proteins can affect their function and it often alters pathogenesis of viral infections. The host protein that I focused on in Chapter I is TBK1. TBK1 is a target for suppression of IFN production by the NSs proteins of SFTSV and HRTV, both of which are human-pathogenic tick-borne bandaviruses. In Chapter II, I focused on a viral protein, EBOV VP35. EBOV is known to be highly pathogenic to humans. VP35 is a multifunctional protein that acts as a viral polymerase cofactor and an interferon antagonist that plays an important role in the pathogenesis of EBOV infection.

In Chapter I, I first compared IFN-producing capacity of TBK1 among various animal species in the presence of the SFTSV NSs protein since it is unclear whether TBK1 of nonhuman animals are also targeted by the SFTSV NSs protein while SFTSV is known to infect various animal species. Interestingly, chicken TBK1-mediated IFN induction was not suppressed by the SFTSV NSs protein whereas the function of TBK1 from other tested mammals including human were uniformly inhibited. These data indicate that chicken TBK1 is resistant to the IFN-inhibitory activity of the SFTSV NSs protein. Next, I focused on genetic polymorphisms in human TBK1. I selected nsSNVs from public database sequences of human TBK1 and investigated the function of TBK1 with the nsSNV substitutions. It was found that some of the nsSNV substitutions in human TBK1 significantly reduced the IFN-inhibitory activity of SFTSV and/or HRTV NSs proteins whereas the magnitude of the effect differed among the nsSNVs. These results suggest that TBK1 polymorphisms may affect the IFN antagonism of the bandavirus NSs proteins and could potentially be one of the factors for differences in the severity of SFTSV and HRTV infections in humans.

In chapter II, the physical properties of the surface of VP35 IID were analyzed, focusing on hydrophobic patches. By patch analysis *in silico*, 3 hydrophobic patches were found on the surface of VP35 IID. Site-directed mutagenesis targeting these 3 hydrophobic patches revealed that disruption of the hydrophobicity of the patches significantly decreased the efficiency of viral genome replication/transcription due to reduced interaction with NP. It was also found that the hydrophobic patches were involved in the IFN-inhibitory function of VP35. These data indicate the importance of hydrophobic patches on the surface of EBOV VP35 IID for the protein functions. It was also demonstrated that patch analysis is a useful tool to identify amino acid residues important for protein functions.

The present study demonstrates that combination of bioinformatics approach (i.e., SNV data and patch analyses) and biological assays is a useful way to identify the molecular determinants that are potentially associated with pathogenesis of virus infections. Although further analyses are needed to clarify the detailed mechanisms how the tested mutants of TBK1 and EBOV VP35 affect their protein functions, the present study advanced my knowledge on the fundamental properties of these proteins. Application of this approach to other viral and host proteins may provide new insights into strategies to develop new therapeutic agents and vaccines.

Acknowledgments

My heartfelt appreciation goes to my supervisor Prof. Ayato Takada (Division of Global Epidemiology, International Institute for Zoonosis Control [IIZC], Hokkaido University [HU]) who offered continuing support and constant encouragement, the continuous support of my research, for his patience, motivation, and immense knowledge. His guidance helped me in all the time of research and writing of this thesis.

I sincerely appreciate the invaluable suggestions and advice from Prof. Hirofumi Sawa (Division of Molecular Pathobiology, IIZC, HU), and Lecturer Dr. Keita Matsuno (Division of Risk Analysis and Management, IIZC, HU), and Associate Prof. Manabu Igarashi (Division of Global Epidemiology, IIZC, HU). Each of you has given advice that has helped me to refine my Ph.D. and expand my research skills.

I would like to specially thank Assistant Prof. Reiko Yoshida, Assistant Prof. Rashid Manzoor, and Assistant Prof. Masahiro Kajihara (Division of Global Epidemiology, IIZC, HU) for their technical and intellectual support. All my gratitude to Ms. Hiroko Miyamoto, Ms. Kanako Ibaraki and Ms. Akina Mori-Kajihara for all their assistance and advice. I would like to thank to all the members of the Division of Global Epidemiology for their kind and heartfelt support.

I am also grateful to thank Dr. Hideaki Ebihara (Department of Virology 1, National institute of infectious Diseases), for their technical support and their provision of important materials (e.g., expression plasmids)

I am grateful to the coordinator at the Program for Leading Graduate Schools, HU, Prof. Motohiro Horiuchi (Laboratory of Veterinary Hygiene, Faculty of Veterinary Medicine, HU), and the members of the Leading Program Office for their help with my Ph.D. coursework.

I would also like to express my gratitude to my family for their moral support and warm encouragements.

Abstract in Japanese

新興感染症の約 60%を占める人獣共通感染症は、地球規模で公衆衛生上の脅威となっている。人獣共通感染症のうち、エボラウイルス（EBOV）病などのウイルス性出血熱は重篤で死亡率の高い疾患である。また、日本でも血小板減少を伴う比較的致死率の高いウイルス性疾患である重症熱性血小板減少症候群（SFTS）が年間 60〜90 例報告されている。EBOV 病や SFTS に対して有効な治療法やワクチンは現在のところ限られている。これらのウイルス感染症の病態を決定する分子メカニズムには、宿主およびウイルス蛋白質の相互作用が深く関わっている。その相互作用を変化させる 1 つのアミノ酸変異でさえも、ウイルスの病原性や感染病態を左右する可能性がある。

第 1 章では、宿主蛋白質 TBK1 の多型に着目した。ヒトに病原性を示すダニ媒介性バンダウイルスである SFTS ウイルス（SFTSV）とハートランドウイルス（HRTV）の非構造（NSs）蛋白質は、インターフェロン（IFN）シグナル経路の TANK-binding kinase 1 (TBK1)を標的として IFN の産生を抑制する。SFTSV は様々な動物種に感染することが知られている一方で、ヒト以外の動物種の TBK1 が NSs 蛋白質の標的となるのか不明であった。そこでまず、NSs 蛋白質の存在下で様々な動物種の TBK1 の IFN 誘導能について比較検討した結果、ヒトを含む他の哺乳類の TBK1 による IFN 誘導は、SFTSV の NSs 蛋白質によって抑制される一方で、ニワトリ TBK1 は抑制を受けないことが分かった。これは、ニワトリの TBK1 が SFTSV の NSs 蛋白質による IFN 阻害活性に対して抵抗性であることを示唆している。次に、ヒトの TBK1 のアミノ酸変異をもたらす一塩基多型（nsSNVs）に着目し、公開データベースからヒト TBK1 の nsSNVs を複数選択した。個々の nsSNVs と同一のアミノ酸置換を導入した変異体 TBK1 を作出し、NSs 蛋白質存在下における IFN 誘導能への影響を調べた。その結果、ヒト TBK1 で報告されている nsSNVs の中には SFTSV や HRTV の NSs 蛋白質の IFN 阻害活性を著しく低下させるものが含まれていること、また nsSNV 変異によって IFN 阻害活性への影響の程度が異なることが明らかになった。これらの結果は、nsSNVs を含む TBK1 の多型がバンダウイルス NSs 蛋白質の IFN 拮抗作用に影響を与え、ヒトにおける SFTSV と HRTV の感染病態に影響を与える因子の 1 つとなる可能性を示唆する。

第２章では、ヒトに対して高い病原性を示すことが知られている EBOV のウイルス構造蛋白質の一つであるポリメラーゼ補因子（VP35）に注目した。VP35 は多機能蛋白質であり、エボラウイルス病の病態に重要な役割を果たす抗 IFN 因子でもある。本研究では、蛋白質の分子表面特性に着目し、コンピュータ計算によるパッチ解析によって、VP35 のインターフェロン抑制に重要なドメイン（IID）の表面に 3 つの疎水性パッチを同定した。そこで、疎水性パッ

チの特性を消失させる部位特異的変異を導入した VP35 を作出し機能を解析したところ、疎水性パッチ変異体では EBOV 核蛋白質（NP）との相互作用が低下し、ウイルスゲノムの転写・複製の効率が有意に低下することが明らかとなった。さらに、それらの変異体は VP35 の IFN 阻害機能をも低下させた。これらの結果は、VP35 IID の表面にある疎水性パッチが本蛋白質の機能にとって重要であることを示している。また、本研究によって、パッチ解析が蛋白質機能に重要なアミノ酸残基を同定するための有用なツールであることが示された。

本学位論文では、遺伝子多型データ解析およびパッチ解析等のバイオインフォマティクスと分子生物学的手法による蛋白質機能解析を組み合わせた研究手法によって、SFTSV、HRTV および EBOV 病の感染病態に関与しうるアミノ酸変異を探索した。TBK1 および VP35 の 1 アミノ酸変異が蛋白質機能に影響を与える詳細なメカニズムの解明にはさらなる解析が必要であるが、本研究によってこれらの蛋白質の基本特性に関する理解が深まった。本手法を他のウイルスや宿主蛋白質に応用することで、治療薬およびワクチン開発戦略に新たな知見をもたらすことが期待される。

References

1. Jones KE, Patel NG, Levy MA, Storeygard A, Balk D, Gittleman JL, Daszak P. 2008. Global trends in emerging infectious diseases. Nature 451:990–993.
2. Taylor LH, Latham SM, woolhouse MEJ. 2001. Risk factors for human disease emergence. Philos Trans R Soc Lond B Biol Sci 356:983–989.
3. Rupasinghe R, Chomel BB, Martínez-López B. 2022. Climate change and zoonoses: A review of the current status, knowledge gaps, and future trends. Acta Trop 226:106225.
4. Kobayashi Y, Kato H, Yamagishi T, Shimada T, Matsui T, Yoshikawa T, Kurosu T, Shimojima M, Morikawa S, Hasegawa H, Saijo M, Oishi K. 2020. Severe fever with thrombocytopenia syndrome, Japan, 2013–2017. Emerg Infect Dis 26:692–699.
5. Robles NJC, Han HJ, Park S-J, Choi YK. 2018. Epidemiology of severe fever and thrombocytopenia syndrome virus infection and the need for therapeutics for the prevention. Clin Exp Vaccine Res 7:43.
6. Muehlenbachs A, Fata CR, Lambert AJ, Paddock CD, Velez JO, Blau DM, Staples JE, Karlekar MB, Bhatnagar J, Nasci RS, Zaki SR. 2014. Heartland virus-associated death in Tennessee. Clin Infect Dis 59:845–850.
7. Schoch CL, Ciufo S, Domrachev M, Hotton CL, Kannan S, Khovanskaya R, Leipe D, Mcveigh R, O'Neill K, Robbertse B, Sharma S, Soussov V, Sullivan JP, Sun L, Turner S, Karsch-Mizrachi I. 2020. NCBI Taxonomy: a comprehensive update on curation, resources and tools. Database (Oxford) 2020.
8. McMullan LK, Folk SM, Kelly AJ, MacNeil A, Goldsmith CS, Metcalfe MG, Batten BC, Albariño CG, Zaki SR, Rollin PE, Nicholson WL, Nichol ST. 2012. A new phlebovirus associated with severe febrile illness in Missouri. N Engl J Med 367:834–841.
9. Kato H, Yamagishi T, Shimada T, Matsui T, Shimojima M, Saijo M, Oishi K. 2016. Epidemiological and clinical features of severe fever with thrombocytopenia syndrome in Japan, 2013–2014. PLoS One 11:e0165207.
10. Fill M-MA, Compton ML, McDonald EC, Moncayo AC, Dunn JR, Schaffner W, Bhatnagar J, Zaki SR, Jones TF, Shieh W-J. 2016. Novel clinical and pathologic findings in a Heartland virus–associated death. Clin Infect Dis 64:510-512.
11. Yu X-J, Liang M-F, Zhang S-Y, Liu Y, Li J-D, Sun Y-L, Zhang L, Zhang Q-F, Popov VL, Li C, Qu J, Li Q, Zhang Y-P, Hai R, Wu W, Wang Q, Zhan F-X, Wang X-J, Kan B, Wang S-W, Wan K-L, Jing H-Q, Lu J-X, Yin W-W, Zhou H, Guan X-H, Liu J-F, Bi Z-Q, Liu G-H, Ren J, Wang H, Zhao Z, Song J-D, He J-R, Wan T,

Zhang J-S, Fu X-P, Sun L-N, Dong X-P, Feng Z-J, Yang W-Z, Hong T, Zhang Y, Walker DH, Wang Y, Li D-X. 2011. Fever with thrombocytopenia associated with a novel Bunyavirus in China. N Engl J Med 364:1523–1532.

12. Santiago FW, Covaleda LM, Sanchez-Aparicio MT, Silvas JA, Diaz-Vizarreta AC, Patel JR, Popov V, Yu X, García-Sastre A, Aguilar P v. 2014. Hijacking of RIG-I signaling proteins into virus-induced cytoplasmic structures correlates with the inhibition of type I interferon responses. J Virol 88:4572–4585.
13. Lee SH, Kim HJ, Byun JW, Lee MJ, Kim NH, Kim DH, Kang HE, Nam HM. 2017. Molecular detection and phylogenetic analysis of severe fever with thrombocytopenia syndrome virus in shelter dogs and cats in the Republic of Korea. Ticks Tick Borne Dis 8:626–630.
14. Niu G, Li J, Liang M, Jiang X, Jiang M, Yin H, Wang Z, Li C, Zhang Q, Jin C, Wang X, Ding S, Xing Z, Wang S, Bi Z, Li D. 2013. Severe fever with thrombocytopenia syndrome virus among domesticated animals, China. Emerg Infect Dis 19:756–763.
15. Xing B, Li X-K, Zhang S-F, Lu Q-B, Du J, Zhang P-H, Yang Z-D, Cui N, Guo C-T, Cao W-C, Zhang X-A, Liu W. 2018. Polymorphisms and haplotypes in the promoter of the TNF-α gene are associated with disease severity of severe fever with thrombocytopenia syndrome in Chinese Han population. PLoS Negl Trop Dis 12:e0006547.
16. Nyakarahuka L, Kankya C, Krontveit R, Mayer B, Mwiine FN, Lutwama J, Skjerve E. 2016. How severe and prevalent are Ebola and Marburg viruses? A systematic review and meta-analysis of the case fatality rates and seroprevalence. BMC Infect Dis 16:708.
17. Wauquier N, Becquart P, Padilla C, Baize S, Leroy EM. 2010. Human fatal Zaire Ebola virus infection is associated with an aberrant innate immunity and with massive lymphocyte apoptosis. PLoS Negl Trop Dis 4:e837.
18. Mühlberger E, Weik M, Volchkov VE, Klenk H-D, Becker S. 1999. Comparison of the transcription and replication strategies of Marburg virus and Ebola virus by using artificial replication systems. J Virol 73:2333–2342.
19. Banerjee A, Pal A, Pal D, Mitra P. 2017. Ebolavirus interferon antagonists-protein interaction perspectives to combat pathogenesis. Brief Funct Genomics 17:392–401.
20. Basler CF, Amarasinghe GK. 2009. Evasion of interferon responses by Ebola and Marburg viruses. J Interferon Cytokine Res 9:511-20.
21. Prins KC, Binning JM, Shabman RS, Leung DW, Amarasinghe GK, Basler CF.

2010. Basic residues within the Ebolavirus VP35 protein are required for its viral polymerase cofactor function. J Virol 84:10581–10591.

22. Leung DW, Ginder ND, Fulton DB, Nix J, Basler CF, Honzatko RB, Amarasinghe GK. 2009. Structure of the Ebola VP35 interferon inhibitory domain. PNAS 106:411-6.
23. Sun Y, Jin C, Zhan F, Wang X, Liang M, Zhang Q, Ding S, Guan X, Huo X, Li C, Qu J, Wang Q, Zhang S, Zhang Y, Wang S, Xu A, Bi Z, Li D. 2012. Host cytokine storm is associated with disease severity of severe fever with thrombocytopenia syndrome. J Infect Dis 206:1085–1094.
24. Hu C, Guo C, Yang Z, Wang L, Hu J, Qin S, Cui N, Peng W, Liu K, Liu W, Cao W. 2015. The severe fever with thrombocytopenia syndrome bunyavirus (SFTSV) antibody in a highly endemic region from 2011 to 2013: A comparative serological study. Am J Trop Med Hyg 92:479–481.
25. Kimura T, Fukuma A, Shimojima M, Yamashita Y, Mizota F, Yamashita M, Otsuka Y, Kan M, Fukushi S, Tani H, Taniguchi S, Ogata M, Kurosu T, Morikawa S, Saijo M, Shinomiya H. 2018. Seroprevalence of severe fever with thrombocytopenia syndrome (SFTS) virus antibodies in humans and animals in Ehime prefecture, Japan, an endemic region of SFTS. J Infect Chemother 24:802–806.
26. Ning Y-J, Wang M, Deng M, Shen S, Liu W, Cao W-C, Deng F, Wang Y-Y, Hu Z, Wang H. 2014. Viral suppression of innate immunity via spatial isolation of TBK1/IKKε from mitochondrial antiviral platform. J Mol Cell Biol 6:324–337.
27. Wu X, Qi X, Qu B, Zhang Z, Liang M, Li C, Cardona CJ, Li D, Xing Z. 2014. Evasion of antiviral immunity through sequestering of TBK1/IKKε/IRF3 into viral inclusion bodies. J Virol 88:3067–3076.
28. Li J, Li J, Miyahira A, Sun J, Liu Y, Cheng G, Liang H. 2012. Crystal structure of the ubiquitin-like domain of human TBK1. Protein Cell 3:383–391.
29. Ikeda F, Hecker CM, Rozenknop A, Nordmeier RD, Rogov V, Hofmann K, Akira S, Dötsch V, Dikic I. 2007. Involvement of the ubiquitin-like domain of TBK1/IKK-i kinases in regulation of IFN-inducible genes. EMBO Journal 26:3451–3462.
30. Qu B, Qi X, Wu X, Liang M, Li C, Cardona CJ, Xu W, Tang F, Li Z, Wu B, Powell K, Wegner M, Li D, Xing Z. 2012. Suppression of the interferon and NF-κB responses by severe fever with thrombocytopenia syndrome virus. J Virol 86:8388–8401.
31. Moriyama M, Igarashi M, Koshiba T, Irie T, Takada A, Ichinohe T. 2018. Two conserved amino acids within the NSs of SFTS phlebovirus are essential for anti-

interferon activity. J Virol JVI.00706-18.
32. Ning YJ, Feng K, Min YQ, Deng F, Hu Z, Wang H. 2017. Heartland virus NSs protein disrupts host defenses by blocking the TBK1 kinase–IRF3 transcription factor interaction and signaling required for interferon induction. J Biol Chem 292:16722–16733.
33. Zhang C, Shang G, Gui X, Zhang X, Bai X, Chen ZJ. 2019. Structural basis of STING binding with and phosphorylation by TBK1. Nature 567:394–398.
34. Sherry ST, Ward MH, Kholodov M, Baker J, Phan L, Smigielski EM, Sirotkin K. 2001. dbSNP: The NCBI database of genetic variation. Nucleic Acids Res 29:308–311.
35. Team RC. 2018. R: A Language and Environment for Statistical Computin. https://www.r-project.org/.
36. Pothlichet J, Burtey A, Kubarenko A V., Caignard G, Solhonne B, Tangy F, Ben-Ali M, Quintana-Murci L, Heinzmann A, Chiche JD, Vidalain PO, Weber ANR, Chignard M, Si-Tahar M. 2009. Study of human RIG-I polymorphisms identifies two variants with an opposite impact on the antiviral immune response. PLoS One 4.
37. Sun Q, Jin C, Zhu L, Liang M, Li C, Cardona CJ, Li D, Xing Z. 2015. Host responses and regulation by NFκB signaling in the liver and liver epithelial cells infected with a novel tick-borne Bunyavirus. Sci Rep 5:11816.
38. Wang Y, Yin Y, Lan X, Ye F, Tian K, Zhao X, Yin H, Li D, Xu H, Liu Y, Zhu Q. 2017. Molecular characterization, expression of chicken TBK1 gene and its effect on IRF3 signaling pathway. PLoS One 12:e0177608.
39. Outlioua A, Pourcelot M, Arnoult D. 2018. The role of optineurin in antiviral type I interferon production. Front Immunol 9.
40. Sasai M, Shingai M, Funami K, Yoneyama M, Fujita T, Matsumoto M, Seya T. 2006. NAK-associated protein 1 participates in both the TLR3 and the cytoplasmic pathways in type I IFN induction. The Journal of Immunology 177:8676–8683.
41. Jacob ST, Crozier I, Fischer WA, Hewlett A, Kraft CS, Vega MA de La, Soka MJ, Wahl V, Griffiths A, Bollinger L, Kuhn JH. 2020. Ebola virus disease Nat Rev Dis Primers 6:13 .
42. Amarasinghe GK, Aréchiga Ceballos NG, Banyard AC, Basler CF, Bavari S, Bennett AJ, Blasdell KR, Briese T, Bukreyev A, Caì Y, Calisher CH, Campos Lawson C, Chandran K, Chapman CA, Chiu CY, Choi KS, Collins PL, Dietzgen RG, Dolja V V., Dolnik O, Domier LL, Dürrwald R, Dye JM, Easton AJ, Ebihara H, Echevarría JE, Fooks AR, Formenty PBH, Fouchier RAM, Freuling CM,

Ghedin E, Goldberg TL, Hewson R, Horie M, Hyndman TH, Jiāng D, Kityo R, Kobinger GP, Kondō H, Koonin E V., Krupovic M, Kurath G, Lamb RA, Lee B, Leroy EM, Maes P, Maisner A, Marston DA, Mor SK, Müller T, Mühlberger E, Ramírez VMN, Netesov S V., Ng TFF, Nowotny N, Palacios G, Patterson JL, Pawęska JT, Payne SL, Prieto K, Rima BK, Rota P, Rubbenstroth D, Schwemmle M, Siddell S, Smither SJ, Song Q, Song T, Stenglein MD, Stone DM, Takada A, Tesh RB, Thomazelli LM, Tomonaga K, Tordo N, Towner JS, Vasilakis N, Vázquez-Morón S, Verdugo C, Volchkov VE, Wahl V, Walker PJ, Wang D, Wang LF, Wellehan JFX, Wiley MR, Whitfield AE, Wolf YI, Yè G, Zhāng YZ, Kuhn JH. 2018. Taxonomy of the order *Mononegavirales*: update 2018. Arch Virol 163:2283–2294.

43. Cross RW, Mire CE, Feldmann H, Geisbert TW. 2018. Post-exposure treatments for Ebola and Marburg virus infections. Nat Rev Drug Discov 17:413–434.
44. Negredo A, Palacios G, Vázquez-Morón S, González F, Dopazo H, Molero F, Juste J, Quetglas J, Savji N, de la Cruz Martínez M, Herrera JE, Pizarro M, Hutchison SK, Echevarría JE, Lipkin WI, Tenorio A. 2011. Discovery of an ebolavirus-like filovirus in europe. PLoS Pathog 7:1–8.
45. Yang X Lou, Tan CW, Anderson DE, Jiang R Di, Li B, Zhang W, Zhu Y, Lim XF, Zhou P, Liu XL, Guan W, Zhang L, Li SY, Zhang YZ, Wang LF, Shi ZL. 2019. Characterization of a filovirus (Měnglà virus) from *Rousettus* bats in China. Nat Microbiol 4:390–395.
46. Messaoudi I, Amarasinghe GK, Basler CF. 2015. Filovirus pathogenesis and immune evasion: Insights from Ebola virus and Marburg virus. Nat Rev Microbiol 13:663–676.
47. Prins KC, Cardenas WB, Basler CF. 2009. Ebola virus protein VP35 impairs the function of interferon regulatory factor-activating kinases IKK and TBK-1. J Virol 83:3069–3077.
48. Reid SP, Cárdenas WB, Basler CF. 2005. Homo-oligomerization facilitates the interferon-antagonist activity of the ebolavirus VP35 protein. Virology 341:179–189.
49. Basler CF, Mikulasova A, Martinez-Sobrido L, Paragas J, Mühlberger E, Bray M, Klenk H-D, Palese P, García-Sastre A. 2003. The Ebola virus VP35 protein inhibits activation of interferon regulatory factor 3. J Virol 77:7945–56.
50. Cardenas WB, Loo Y-M, Gale M, Hartman AL, Kimberlin CR, Martinez-Sobrido L, Saphire EO, Basler CF. 2006. Ebola virus VP35 protein binds double-stranded RNA and inhibits alpha/beta interferon production induced by RIG-I signaling. J

Virol 80:5168–5178.
51. Hartman AL, Towner JS, Nichol ST. 2004. A C-terminal basic amino acid motif of Zaire ebolavirus VP35 is essential for type I interferon antagonism and displays high identity with the RNA-binding domain of another interferon antagonist, the NS1 protein of influenza A virus. Virology 328:177–184.
52. Leung DW, Prins KC, Borek DM, Farahbakhsh M, Tufariello JM, Ramanan P, Nix JC, Helgeson LA, Otwinowski Z, Honzatko RB, Basler CF, Amarasinghe GK. 2010. Structural basis for dsRNA recognition and interferon antagonism by Ebola VP35. Nat Struct Mol Biol 17:165–172.
53. Prins KC, Delpeut S, Leung DW, Reynard O, Volchkova VA, Reid StP, Ramanan P, Cardenas WB, Amarasinghe GK, Volchkov VE, Basler CF. 2010. Mutations abrogating VP35 interaction with double-stranded RNA render Ebola virus avirulent in Guinea Pigs. J Virol 84:3004–3015.
54. Hartman AL, Bird BH, Towner JS, Antoniadou Z-A, Zaki SR, Nichol ST. 2008. Inhibition of IRF-3 activation by VP35 is critical for the high level of virulence of Ebola virus. J Virol 82:2699–2704.
55. Jones S, Thornton JM. 1997. Analysis of protein-protein interaction sites using surface patches. J Mol Biol 272:121–132.
56. Jones S, Thornton JM. 1997. Prediction of protein-protein interaction sites using patch analysis. J Mol Biol 272:133–143.
57. Niwa H, Yamamura K, Miyazaki J. 1991. Efficient secletion for high-expression transformants with a novel eukaryotic vector. Gene 108:193–199.
58. Kondoh T, Manzoor R, Nao N, Maruyama J, Furuyama W, Miyamoto H, Shigeno A, Kuroda M, Matsuno K, Fujikura D, Kajihara M, Yoshida R, Igarashi M, Takada A. 2017. Putative endogenous filovirus VP35-like protein potentially functions as an IFN antagonist but not a polymerase cofactor. PLoS One 12:1–17.
59. Watanabe S, Noda T, Halfmann P, Jasenosky L, Kawaoka Y. 2007. Ebola virus (EBOV) VP24 inhibits transcription and replication of the EBOV genome. J Infect Dis 196:S284–S290.
60. Watanabe S, Watanabe T, Noda T, Feldmann H, Jasenosky LD, Takada A, Kawaoka Y. 2004. Production of novel Ebola virus-like particles from cDNAs : an alternative to Ebola virus generation by reverse genetics. J Virol 78:999–1005.
61. Changula K, Yoshida R, Noyori O, Marzi A, Miyamoto H, Ishijima M, Yokoyama A, Kajihara M, Feldmann H, Mweene AS, Takada A. 2013. Mapping of conserved and species-specific antibody epitopes on the Ebola virus nucleoprotein. Virus Res 176:83–90.

62. Kimberlin CR, Bornholdt ZA, Li S, Woods VL, MacRae IJ, Saphire EO. 2010. *Ebolavirus* VP35 uses a bimodal strategy to bind dsRNA for innate immune suppression. Proc Natl Acad Sci U S A 107:314–319.
63. Haasnoot J, De Vries W, Geutjes EJ, Prins M, De Haan P, Berkhout B. 2007. The ebola virus VP35 protein is a suppressor of RNA silencing. PLoS Pathog 3:0794–0803.
64. Becker S, Rinne C, Hofsäß U, Klenk HD, Mühlberger E. 1998. Interactions of Marburg virus nucleocapsid proteins. Virology 249:406–417.
65. Marnolia A, Toepak EP, Tambunan USF. 2018. Fragment-based lead compound design to inhibit Ebola VP35 through computational studies. Int J of GEOMATE 15:65–71.
66. Zhang YJ, Ding JN, Zhong H, Sun CP, Han JG. 2017. Molecular dynamics exploration of the binding mechanism and properties of single-walled carbon nanotube to WT and mutant VP35 FBP region of Ebola virus. J Biol Phys 43:149–165.
67. Brown CS, Lee MS, Leung DW, Wang T, Xu W, Luthra P, Anantpadma M, Shabman RS, Melito LM, MacMillan KS, Borek DM, Otwinowski Z, Ramanan P, Stubbs AJ, Peterson DS, Binning JM, Tonelli M, Olson MA, Davey RA, Ready JM, Basler CF, Amarasinghe GK. 2014. *In silico* derived small molecules bind the filovirus VP35 protein and inhibit its polymerase co-factor activity. J Mol Biol 426:2045–2058.
68. Ramanan P, Edwards MR, Shabman RS, Leung DW, Endlich-Frazier AC, Borek DM, Otwinowski Z, Liu G, Huh J, Basler CF, Amarasinghe GK. 2012. Structural basis for Marburg virus VP35-mediated immune evasion mechanisms. Proc Natl Acad Sci U S A 109:20661–20666.
69. Feagins AR, Basler CF. 2015. Lloviu virus VP24 and VP35 proteins function as innate immune antagonists in human and bat cells. Virology 485:145–152.
70. Williams CG, Gibbons JS, Keiffer TR, Luthra P, Edwards MR, Basler CF. 2020. Impact of Měnglà virus proteins on human and bat innate immune pathways. J Virol 94.